Developing a Novel Ultrafine Coal Dewatering Process

Michael H Huylo

Thesis submitted to the faculty of the

Virginia Polytechnic Institute and State University

in partial fulfillment of the requirements for the degree of

Master of Science

In

Mechanical Engineering

Rui Qiao, Chair

Roe-Hoan Yoon

Aaron Noble

Yang Liu

December 3, 2021

Blacksburg, Virginia

Keywords: hydrophobic-hydrophilic separation, coal beneficiation, solvent recovery, steam drying.

Developing a Novel Ultrafine Coal Dewatering Process

Michael H Huylo

Abstract

Dewatering fine coal is needed in many applications but has remained a great challenge. The hydrophobic-hydrophilic separation (HHS) method is a powerful technology to address this problem. However, organic solvents in solvent-coal slurries produced during HHS must be recovered for the method to be economically viable. Here, the experimental studies of recovering solvents from pentane-coal and hexane-coal slurries by combining liquid-solid filtration and in-situ vaporization and removing the solvent by a carrier gas (i.e., drying) are reported. The filtration behaviors are studied under different solid mass loading and filtration pressure. It is shown that using pressure filtration driven by 20 psig nitrogen, over 95% of solvents by mass in the slurries can be recovered, and filtration cakes can be formed in 60 s. The drying behavior was studied using nitrogen and steam at different temperatures and pressures. It is shown that residual solvents in filtration cakes can be reduced below 1400 ppm within 10 s by 15 psig steam superheated to 150°C, while other parameter combinations are far less effective in removing solvents. Physical processes involved in drying and the structure of solvent-laden filtration cakes are analyzed in light of these results.

Developing a Novel Ultrafine Coal Dewatering Process

Michael H Huylo

General Audience Abstract

Coal particles below a certain size are discarded to waste tailing ponds as there is no economically viable method for processing them. However, a new process called hydrophobic-hydrophilic separation offers a solution to this problem. A hydrophobic solvent is used to displace water from a coal-water slurry, and it is then easier and cheaper to filter and dry this new coal-solvent slurry. In this work experimental studies of recovering solvents from pentane-coal and hexane-coal slurries by combining filtration and drying are reported. The filtration behaviors are studied under different solid mass loading and filtration pressures. It is shown that using pressure filtration driven by 20 psig nitrogen, over 95% of solvents by mass in the slurry can be recovered, and filtration cakes can be formed in 60 s. The drying behavior was studied using nitrogen and steam at different temperatures and pressures to evaporate any remaining solvents. It is shown that the remaining solvents in filtration cakes can be reduced below 1400 ppm within 10 s by using 15 psig steam superheated to 150°C as a drying medium, while other parameter combinations are far less effective in removing solvents. Physical processes involved in drying and the structure of solvent-laden filtration cakes are analyzed in light of these results.

Acknowledgement

I would like to thank my three co advisors Dr. Qiao, Dr. Yoon, and Dr. Noble for all of their guidance and support. I am especially grateful to Dr. Qiao for serving as my primary advisor. I am thankful for the opportunity to have been hired as a graduate research assistant, and to have been able to work on this project. I would also like to thank Dr. Liu for serving on my committee.

Additionally, I appreciate all the assistance I received in performing my research from Dr. Kaiwu Huang, Dr. Serhat Keles, Jim Reyher, Dr. Mehdi Ashraf-Khorassani, Glen Brock, and Chad Sechrist.

Thank you to my friends and lab mates Dr. Hai Wu, Seokgyun Ham, David Moh, Hongwei Zhang, Jacob Wilson, Xin Wang, and Mehran Islam for their support, collaboration, and companionship.

Thank you to my mother, sister, and brother for their support and my father for his guidance in the engineering profession.

The support of the United States Department of Energy, National Energy Technology Laboratory through NETL-Penn State University Coalition for Fossil Energy Research (UCFER, contract number DE-FE0026825) is gratefully acknowledged.

Contents

List of Figures

List of Tables

Chapter 1. Introduction

Coal has been a significant source of energy production in the United States for centuries. Widely available and relatively cheap, it was the dominant domestic fuel source for electricity production until being surpassed by natural gas in the last five years. Total coal consumption in the U.S. has fallen from 1 billion short tons in 2010 to less than 500 million short tons in 2020 [1]. However, coal continues to produce more electricity in the U.S. than renewables or nuclear sources. While electricity generated from coal is projected to decrease as a percentage of overall energy generated, the rapid increase in world energy generation will allow overall coal use to remain relatively consistent [1]. In addition to this, the market for high-quality metallurgical coal is growing. Metallurgical coal is required for coke production and steelmaking processes. Therefore, there continues to be demand for high-quality coal production, and the industry remains worthy of technological investment as far as remediating waste and environmental hazards [1].

As coal mining developed from underground miners and carts to high-volume large machinery, the quality and particle size of the coal produced has decreased. This has resulted in the need for more efficient processing and cleaning. Raw coal removed from the ground contains many impurities that must be removed, and this removal process can be achieved in many ways depending on particle size.

Larger particles can be separated from impurities based on differences in density. Medium size to smaller particles can be separated using cyclones, bed separators, or spirals. The smallest and most challenging to process particles require using flotation cells. This usually involves using air bubbles injected into a water tank to carry coal particles to the surface where they can be extracted. The waste particles are left behind at the bottom of the tank. The smallest particles, typically below

40 microns, are rejected to waste because there is no economically effective means of processing them. As of 2002, 70-90 million tons of small and fine coal tailings were produced in the U.S. each year but discarded due to the difficulties of dewatering them [3]. The discarded fine coal not only causes a significant economic loss but also creates environmental pollution concerns. As of 2002, it was believed that there might be up to 2 billion tons of ultra-fine slurry located in waste tailing ponds [3]. While overall coal production has slowed since 2002, the total mass stored in tailing ponds has only increased.

In addition to waste minerals and particles that must be removed, moisture is also considered a contaminant. This becomes even more problematic when dealing with flotation-sized particles because they are immersed in water in the flotation tank. The excess water then becomes very difficult and expensive to filter and evaporate, as described later in this section.

Dewatering of particulate materials is an essential operation not only in coal, but nearly all other mined commodities. Further, other diverse applications such as pharmaceutical manufacturingalso require dewatering. Unfortunately, existing dewatering techniques often suffer from high cost, low scalability, and low efficiency. Consequently, many industries are still significantly hindered by the lack of effective dewatering technologies. For example, in coal mining, coal particles less than 1 mm in size account for approximately 10% of the total product but can contain more than one-third of the total moisture [5].

Presently, there are two main strategies to dewater fine coal. One is to thermally evaporate water using fluidized beds, multi-louvered systems, or flash-type systems [6]. These methods are often costly and can produce fugitive dust and toxic elements that can escape into the environment. Indeed, it has become difficult to obtain permits for thermal dryers in the U.S. due to environmental requirements [2]. While thermal dryers can provide a dry final product (moisture <10%), coking

properties of coal are negatively affected, and the energy and installation cost make the drying process economically inviable except in rare circumstances. Usually, the dryers operate using convection via hot combustion gases to dry wet fine coal products.

The other strategy is to use mechanical means such as filters and centrifuges. The mechanical approach is inefficient due to the high pressures needed. According to Poiseuille's equation, which governs fluid flow through a filter cake, a ten-fold decrease in pore size (and thus particle size) would require a 10^4-times increase in pressure drop (ΔP) across coal filtration cakes to obtain the same dewatering rate. In effect, mechanical dewatering has reached its limit, which is partly why the industry continues to discard coal fines to impoundments. It is apparent that pressure filtration is not viable for dewatering very small coal particles, and a new method is needed.

Recently, a team in the Mining and Minerals Engineering department at Virginia Tech developed a novel dewatering and cleaning process known as hydrophobic-hydrophilic separation (HHS), which has no lower particle size limit in solid-solid separation and produces practically dry coal in solid-liquid separation [7-9]. To begin the HHS process, a nonpolar solvent, typically short-chain alkanes with low surface tension and boiling point (e.g., liquid hexane), is introduced to a water-coal slurry. This causes the coal particles to move from an aqueous phase to a solvent phase.

The transfer of hydrophobic particles from the water phase to the organic solvent phase is thermodynamically spontaneous and depends on surface tensions, contact angles, etc. Mechanical mixing can be introduced to accelerate the water-solvent phase change process. Calculations for the adsorption of a hydrophobic particle to the oil-water interface are similar to the adsorption of a hydrophobic particle to an air bubble, as used in froth flotation. However, the greater contact

angle provided by the oil-solid interface leads to HHS being more effective at coal cleaning than air bubble froth flotation [2].

Some coal particles will transfer from the aqueous phase to the solvent phase as independent particles. However, there will be remaining agglomerations that have trapped water droplets. This phenomenon requires using a reactor to vibrate the mixture and free any trapped water droplets. Once the particles are entirely in the solvent phase, the water and solvent are separated by gravity. The replacement of the water with solvent is not dependent on particle size. Therefore the cost of dewatering does not grow exponentially as particle size decreases, which has plagued current technologies.

Next, solvents are recovered from the solvent-coal slurry. To recover the solvents, a filtration step is used first (see Figure 1a). Here, the slurry is placed above a porous filter, and an inert gas is used to drive solvents through the filter. As the gas displaces liquid solvents, a filtration cake gradually forms on the filter. Due to the high gas pressure, liquid solvents are driven through the cake continuously until the gas breaks through the filtration cake. The filtration rate is determined by pressure drop, capillary pressure of solvents within the cake structure, and solvent viscosity (see Eq. 2 in Section 3.1) [10]. In past HHS experiments, N_2 has been used to drive filtration [11, 12]. At the end of the filtration step, most of the solvent initially present in the solvent-coal slurry can be recovered. However, some residual solvents remain trapped inside the filtration cake. Because solvents are expensive, these residual solvents must be recovered for the HHS technology to be economically viable.

At present, HHS experiments have utilized thermal dryers with electrically powered screw conveyors to vaporize and recover the residual solvents. These have proven to be very effective at removing solvents from the filtration cake. However, they are not ideal when scaled up for pilot

plant or commercial use due to their high equipment and installation costs, as well as difficulties in integrating with the equipment for filtration of solvent-coal slurries. It is necessary to develop a more efficient means of evaporating spent solvent to commercialize the HHS process.

It would be ideal to develop an in-situ solvent recovery scheme that integrates the above liquid-solid filtration step with a solvent vaporization and removal step in a single device. Following the first filtration step shown in Figure 1a, a second step is introduced: a carrier gas is pumped through the filtration cake to vaporize and remove the residual solvents (see Figure 1b). The second step is hereafter referred to as the drying step. The envisioned scheme will allow significant equipment savings and easy integration into existing filter systems. Potentially useful carrier gas includes nitrogen, heated nitrogen, and superheated steam. This is due to the gases being inert, and is based on previous HHS work conducted by other students. The speed and effectiveness of the solvent recovery in the second step depend critically on the distribution of liquid solvents inside the filtration cake. After gas break through, the distribution of nonpolar liquids in a porous cake with micron-sized, complex-shaped particles is not well understood yet. There are two possible limiting scenarios (see Figure 1b). In the first scenario, the residual solvents form a continuous film spanning across the surface of carrier gas pathways. In the second scenario, the residual solvents exist as isolated clusters that are sparsely dispersed in the filtration cake. Solvent recovery is expected to be facile in the first scenario but more difficult in the second scenario.

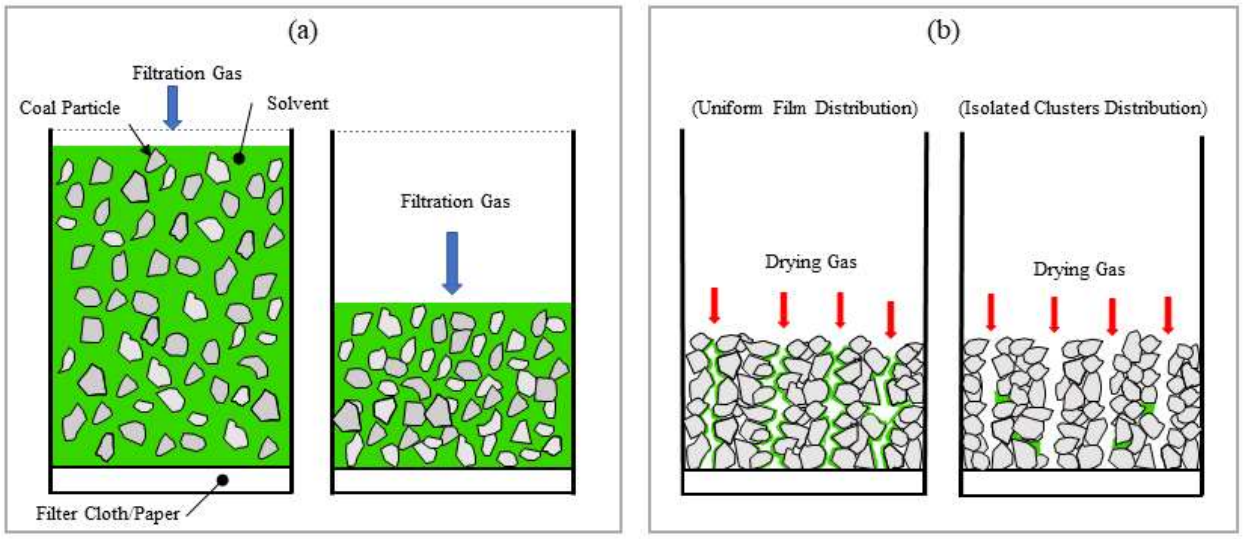

Figure 1: Two-step, *in-situ recovery of nonpolar solvents from solvent-coal slurries*. In Step I, an N_2 gas drives solvents through a filter paper/cloth, forming a filtration cake (panel a). In Step II, which starts after the gas breaks through the filtration cake, a carrier gas is pumped through the cake to vaporize and remove the residual solvents (panel b). The schematics in (b) show two limiting scenarios that are possible for the distribution of residual liquid solvents (colored in green) at the beginning of Step II.

Previous drying studies of porous materials display some characteristic behaviors. Typically, drying occurs in two stages. First, there is a "Constant Rate Period", where moisture content of a sample decreases linearly with time. This stage ends when moisture reaches a point called the "Critical Moisture Content". Upon reaching this point, the drying rate changes to the second stage, the "Falling Rate Period". Here, the drying rate continues to decrease until reaching zero at the point where sample moisture reaches an equilibrium state with the drying medium [13, 14]. The behavior of solvent removal from a porous particle cake driven by a carrier gas has not been studied previously, and it is unknown if these same characteristics occur.

It is the goal of this work to experimentally investigate the envisioned in-situ solvent recovery scheme. The operation of this scheme involves many parameters such as filtration pressure, solid loading in slurry, and type, pressure, and temperature of the carrier gas. These parameters will be explored to determine solvent recovery efficacy. Because the envisioned scheme is intended for

integration with the HHS technology, slurry filtration should take no longer than sixty seconds, and solvent vaporization should take no longer than ten seconds. In addition, the solvent concentration in filtration cakes must be reduced below 1400 ppm, which is typical of that obtained in commercial thermal dryers.

The rest of this thesis is organized as follows. Chapter 2 presents the experimental setup, materials, and methods for filtration experiments and solvent vaporization (drying) experiments. Chapter 3 presents the results from these experiments and insight into the optimization of in-situ solvent recovery scheme. The likely distribution of solvents inside filtration cakes will be deduced from the experimental data. Finally, conclusions are drawn in Chapter 4.

Chapter 2. Materials, Experiment Setup, and Methods

In the *in-situ* solvent recovery scheme shown in Figure 1, most of the solvent is recovered from the slurry during the filtration stage. Only a small remaining portion is removed from the filtration cake via vaporization during the drying stage. To simulate the in-situ solvent recovery process in laboratory experiments, first, a slurry was prepared and poured into a pressure cylinder. Next, a filtration cake was formed by pressure filtration, during which liquid solvent was recovered. Last, any residual solvent in the filtration cake was vaporized and carried out of the filtration cake by a drying gas stream. Experiments were performed for both the filtration and drying stages, and the experimental details are provided in this section.

2.1 Materials

The coal was originally prepared from a screen bowl effluent in a commercial plant. The as-received material was processed through a pilot-scale HHS plant housed in the VT Mining and Minerals Engineering research facility. The particle size distribution of the clean coal sample was found from using a Microtrac particle characterization analyzer. A small sample of several grams was loaded into the machine and the percentiles were determined from light scattering technology. The coal sample has a D_{80} particle size of 43.25 μm. The overall particle size distribution for the sample is displayed in Table 1. Additionally, Figure 2 shows a cumulative line plot of the particle size distribution.

Table 1: Coal sample size distribution.

Percentile (%)	Size (µm)
10.00	1.228
20.00	3.15
30.00	6.02
40.00	9.12
50.00	13.09
60.00	19.55
70.00	28.84
80.00	43.25
90.00	84.90
95.00	198.6

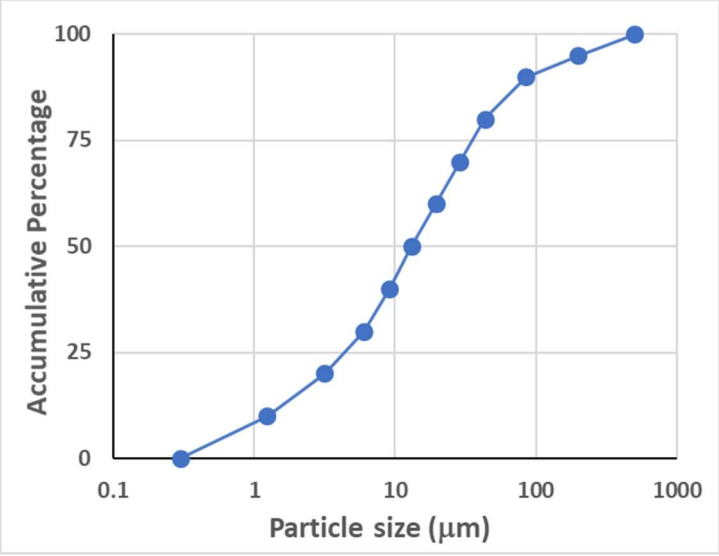

Figure 2: A cumulative percentage curve for the particle size in the experimental coal sample.

Hexane was chosen as the primary solvent to be evaluated for this work. Pentane was also evaluated to serve as a reference. Relevant properties of these solvents are shown in Table 2.

Table 2: Properties of solvents used in this work at 20 °C and 1 atm.

Solvent	Density (g/cm^3)	Viscosity (mPa·s)	Boiling point (°C)	Vapor pressure (kPa)
Pentane	0.626	0.250	36.0	57.3
Hexane	0.659	0.310	69.0	16.0

2.2 Filtration tests

2.2.1 Experimental Setup and Methods

Filtration tests were performed to determine a reasonable filtration pressure. In these tests, nitrogen (N_2) gas was used because our solvents are combustible. In most tests, pressure filtration was conducted using pressurized N_2 to displace liquid solvents from the coal slurries. It is desirable to use low applied pressure as the energy cost of filtration rises sharply with increasing pressure. However, reducing the applied pressure increases filtration time and decreases the throughput in practical operations. Table 3 summarizes the filtration pressure and other filtration parameters used in the filtration tests.

Table 3: Conditions for the pressure filtration kinetics experiments.

Solvent	Pressure (psig)	% Solids by weight	Coal Mass (g)
Pentane	20, 40, 60	10, 15	25
Hexane	20, 40 ,60	10, 15	25

Before the filtration experiments, a coal slurry was prepared. 25 g of coal are weighed on a mass balance. Next, the necessary solvent volume is measured in a graduated cylinder based on the target solid weight fraction of the slurry (10% and 15% were adopted in this study). As required by the HHS process, the solvent is typically hydrophobic hydrocarbons. To be viable for pilot plant use and later commercial use, the solvent must have a relatively low viscosity so that filtration can be performed rapidly while not being overly volatile due to safety considerations. Next, the coal was placed into a glass beaker with a magnetic stir bar and the solvent was poured over it. The solution was mixed on a magnetic stir plate for 8 minutes before use in the filtration tests.

Figure 3 shows the schematic of the apparatus assembled for measuring solvent filtration kinetics. The apparatus consists of a pressure filtration cylinder, a filter cloth and paper, a solvent collection beaker, and a mass balance. The cylinder measures 8 in. high, and has a 2.5-in. ID and 3.5-in. OD. At the top of the cylinder there is a 0.25-in. inlet where the nitrogen was injected. At the base of the cylinder were a filter cloth and a 5-micrometer filter paper used to form a particle cake. Downstream of the filter cloth/paper was the bottom cover, and it has a 0.25-in. plastic outlet hose, which directed the filtered solvent into a glass Erlenmeyer flask resting on a mass balance. The mass balance was connected to a computer with data logging software, which recorded the solvent collected every 0.2 seconds. The resulting data was used to develop filtration plots.

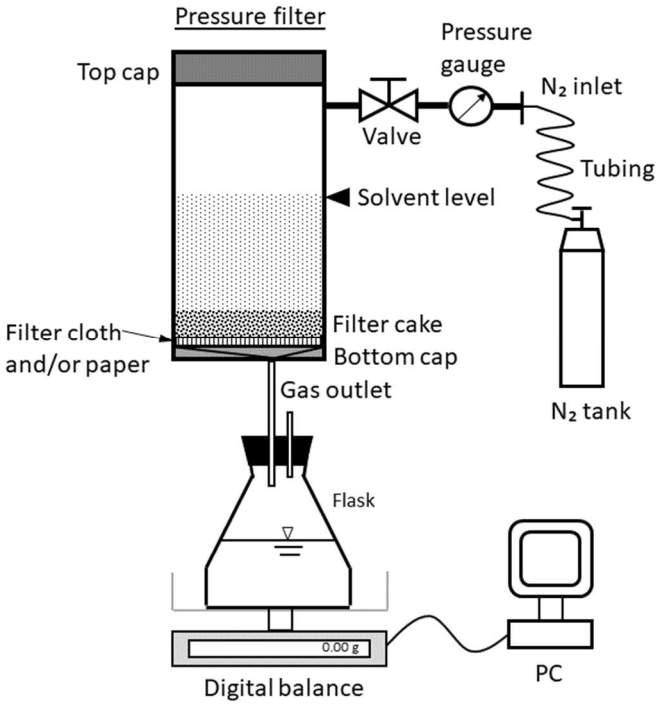

Figure 3: A schematic of the pressure filtration apparatus for recovering liquid solvent from a coal slurry.

In each filtration run, a clean filter paper was installed into the bottom of the cylinder above the fluid outlet. Next, a homogeneous solvent-coal slurry was poured into the pressure cylinder, and the cylinder top cap was sealed. Nitrogen delivery pressure was set, and the nitrogen valve was opened to initiate the filtration test. Filtration continued until the gas broke through the filter cake. Figure 4 is a photograph of the filtration testing setup in the mining laboratory.

Figure 4: A photo of the filtration testing setup.

In Figure 4 the mixing beaker is shown on the left side of the photo. It is located on top of the magnetic stir plate, and a stir bar is inside of the slurry in the beaker. The pressure filter is located on the right side of the photo in the fume hood. The top cap is removed and located on the left. Yellow coiled nitrogen gas tubing is to the right of the cylinder, and is connected to a nitrogen reservoir tank located outside of the photo. In front of the hood the solvent collection beaker is placed on top of a balance. A cable runs from the balance to a laptop is not shown in the photo. The laptop utilizes software to record the amount of solvent collected versus time. Figure 5 is a photo of a coal cake after it was removed from the cylinder at the completion of filtration.

Figure 5: A coal cake removed from the pressure filtration cylinder after the completion of an experiment.

In addition to the pressure filtration presented above, one vacuum filtration test was also conducted. For large-scale, commercial applications, vacuum filtration is often more economical than pressure filtration. It is thus useful to determine whether a filtration cake formed by high-pressure nitrogen filtration dries differently than that of a cake formed by vacuum filtration. To accommodate vacuum testing, the tube at the discharge of the cylinder was connected to a vacuum pump inlet. A second tube was run from the vacuum pump outlet to the collection beaker. Below is the detailed step by step procedure for conducting the filtration testing.

2.2.2 Experimental Procedure

1. Prepare the coal-solvent slurry by weighing ten or fifteen percent by mass coal sample;
2. Pour the ninety percent or eighty five percent by mass solvent into the mixing vessel with the coal sample;
3. Place mixing vessel on the mixing plate for eight minutes and cover with glass dish to prevent splashing and unwanted evaporation;

4. Place the collection beaker onto the digital balance;
5. Prepare the mass balance analysis software on the connected laptop;
6. Place a new single use filter paper onto the reusable filter cloth and install both on the bottom screw cap of the pressure filter;
7. Connect the nitrogen hose to the top of the pressure filter;
8. Set the desired nitrogen delivery pressure on the pressure gauge;
9. Wait until the eight-minute mixing time has been reached;
10. Turn off the mixing plate;
11. Remove the mixing vessel from the plate and pour the slurry into the pressure vessel;
12. Place the top screw cap onto the cylinder and tighten;
13. Start the mass balance software on the laptop;
14. Open the nitrogen shutoff valve;
15. Inject nitrogen into the pressure cylinder until the gas has broken through the cake and there is no more solvent flow into the collection beaker;
16. Turn off the nitrogen shutoff valve;
17. Turn off the mass balance software;
18. Save the mass balance file with the appropriate pressure, solvent, and solids percentage;
19. Remove the bottom screw cap;
20. Dispose of the cake sample and paper filter;
21. Remove the top screw cap;
22. Clean the inside of the cylinder with water and disposable towel;
23. Wait until the solvent and cylinder has returned to room temperature before performing another trial;

2.3 Solvent vaporization and removal tests

As seen in Figure 1 in the introduction, the solvent trapped in micro-capillaries is difficult to remove by filtration. Instead, the residual solvent in the particle cake formed via filtration must be vaporized and then flushed out of the cake by a carrier gas. A key parameter of this process is the choice of carrier gas. Options for solvent vaporization mediums in HHS are limited to those preventing combustion. Two potentially feasible options are nitrogen and superheated steam, both of which have relative advantages and disadvantages.

Nitrogen is easy to work with and requires fewer design considerations than superheated steam. A nitrogen reservoir tank along with a pressure gauge/controller and some plastic tubing are all that is needed to deliver nitrogen gas for drying. However, it has a lower heat capacity and may require very high delivery temperatures, or very high gas flow rates which lead to high required pressures for drying.

Steam has a higher heat capacity, and at similar pressures and temperature, may provide faster drying. When drying with superheated steam, several physical processes are involved. First, the coal cake to be dried will have its temperature raised to the saturation temperature of the steam. As this happens, some of the steam will condense on the coal and the surfaces of the drying vessel. Meanwhile, the solvent in the cake is vaporized. Once the material has reached the steam saturation temperature, the condensed water evaporates back into the superheated steam. The condensation from the superheated steam and re-evaporation of condensed water allows this method to control both the solvent content and water content in the dried coal. This is advantageous because if the coal is too dry, it poses a safety hazard during transportation. The disadvantages of superheated steam are that it requires a more complicated production process and added considerations for

dealing with condensate, among other issues. Both nitrogen and superheated steam will be tested as part of this work.

Superheated steam-based drying is a well-studied, developed technology used in other drying industries. It is frequently utilized in drying food, grains, and minerals [16-25]. Existing steam drying works have several differences from this work. Most use superheated steam to dry products containing water, but not organic solvent. Additionally, most works focused on drying using fluidized beds, impingements jets, rotary drums, or belt systems as opposed to a pressure cylinder [17, 20-23, 25, 26]. The process studied here is unique in that vaporization is step two of a two-part solvent recovery method. Therefore, drying is conducted in the same vessel used for filtration in step one; superheated steam flows through the material to be dried (coal cake), and the drying product remains in contact with the pressure vessel enclosure.

2.3.1 Experimental Apparatus Preliminary Design

The apparatus shown in Figure 3 was modified so that it can be used to perform both filtration and solvent vaporization and removal. A preliminary design for the modification of the apparatus is shown in Figure 6.

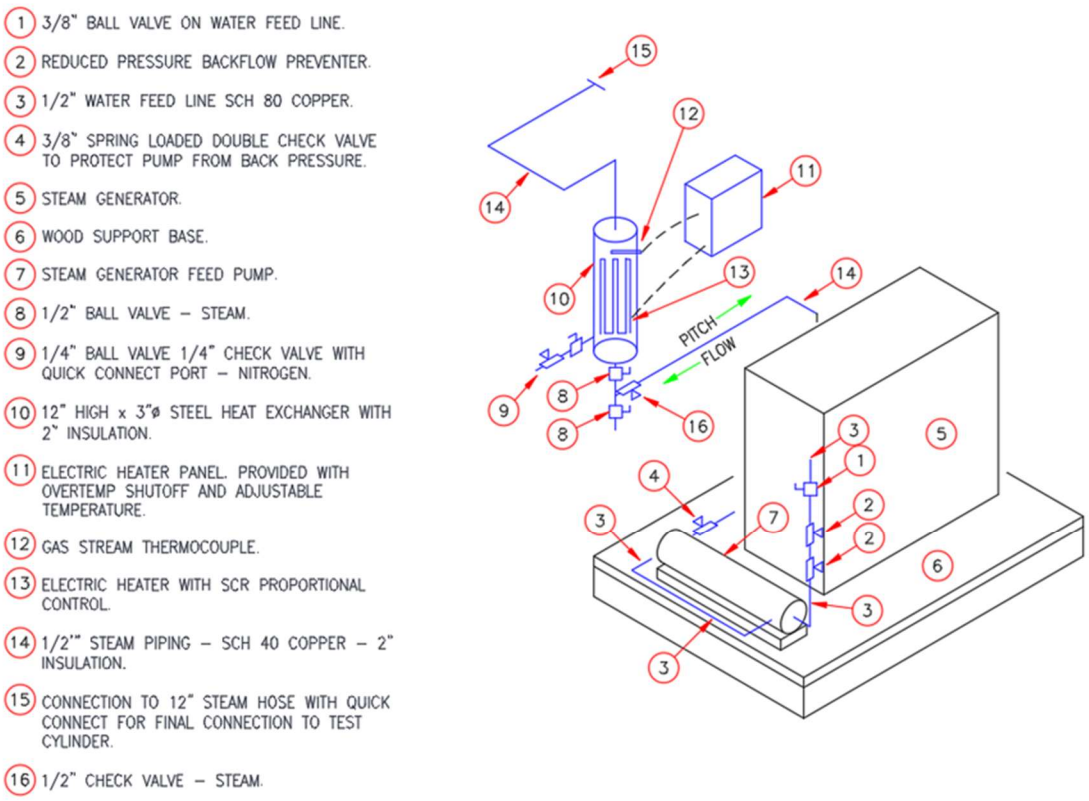

Figure 6: A preliminary design schematic of modifications to the filtration equipment to accommodate nitrogen filtration, nitrogen drying, heated nitrogen drying, and superheated steam drying.

Initially the preliminary design shown in Figure 6 was given to several contractors and equipment suppliers to be competitively bid. After receiving bids, it was determined that some changes would need to be made to this design to be within the project's financial budget. Careful decisions were made to allow cost reduction without drastically reducing the quality and accuracy of the proposed experiments. Originally, it was desired to purchase a factory-made heat exchanger with a factory provided heating source and controls as shown in number thirteen and number eleven in Figure 6. This item alone was worth twice as much as the steam boiler itself and a decision was made to remove it from the proposed system. In its place, a plate heat exchanger, and electrical heating tape with a thermostat were purchased separately. This reduced the cost by a

factor of twenty and still allowed accurate temperature control. Thermocouples were added upstream, downstream, and within the plate itself to provide both temperature control and monitoring. Later in this section, calculations are provided to select both the heat exchanger length, and the output power of the electrical heating tapes.

The boiler feedwater design proved to be an additional cost issue. Connecting to the building water supply piping required the work of a licensed plumber and purchasing additional backflow safety valving to satisfy local building code requirements. It was determined that it would be cheaper and more effective to use a small water reservoir to provide feed water to the boiler. It was anticipated from previous data that drying should not take longer than sixty seconds. Given that the boiler reservoir can be set to eighty psig, and is then regulated to a lower pressure downstream, many trials can be run before the feed pump needs to turn on and refill the boiler. Later when this system is scaled up to a pilot plant, or commercial use, a constant water supply from a building source will be required, but that is not the case for bench scale experiments. Last, before finalizing this change, it was verified that the boiler feedwater pump's net positive suction head was below that of the head provided by atmospheric pressure.

Two options are presented when purchasing a steam boiler. The boiler heating source can be electrically powered, or it can generate steam through the burning of natural gas or some other fuel. For large scale commercial use the energy savings would necessitate the use of a gas boiler, but at the bench scale an electric boiler offers several conveniences. First, there are no products of combustion that require venting with an electric boiler. Due to the location of the lab where these experiments will be performed, venting products of combustion to the outdoors could cost upwards of ten thousand dollars. Second, an electric boiler does not require installing natural gas valving, piping, and burner controls. It is far cheaper and more convenient to purchase an electric boiler

and use a twenty-foot flexible power cable. These advantages lead to the decision to choose the electric boiler option.

Due to the relatively small flow rate of steam required to dry such a small sample, it was a safe assumption that the smallest available boiler in the product line would have an adequate capacity. However, a precautionary flow rate test was performed to provide verification. A gas flow rate measuring device was acquired, and two tests were run to determine the flow rate of nitrogen through a completely formed particle cake. At 15 psig the flow rate was 15,000 sccm (standard cubic centimeter per minute.). Knowing the viscosity of nitrogen and steam, it is possible to roughly predict the flow rate of steam at 15psig, and the result is 13,700 sccm. Multiplying this flowrate by the density of 15 psig superheated steam, it is found that no more than 1 kg/hr of steam should be required for drying the experimental coal cake. The smallest available electric boiler produces approximately 4kg/hr, and therefore will be adequate. The electric steam boiler that was purchased for the experiments is shown in Figure 7. It was delivered on a wood pallet and included with a boiler water feed pump.

Figure 7: The electric steam boiler purchased for use in the drying experiments.

The purchased steam boiler was delivered with a 120-volt single phase boiler feed pump and a pressure control system ranging from 0 to 100 psig. The boiler feed pump can be plugged into a traditional wall outlet. The electric heating source itself is 480-volt 3 phase and will need to be wired by an electrician. After the steam boiler was purchased, it was necessary to determine the heat exchanger length required for superheating the steam and heating the nitrogen gas.

Given that an estimated flow range was determined from experimental measurement, this value was used to calculate the required length of the heat exchanger used to superheat the steam and heat the nitrogen. The heat exchanger chosen was a copper tube that makes several passes through a steel plate. The plate itself is heated to a required temperature by an electric heating tape with a thermostat control. Assuming the plate will have a uniform temperature, and that the copper tube inside the plate has a uniform wall temperature, a calculation can be performed to determine

the length required to raise the temperature of the fluid flowing through the exchanger to near the temperature of the pipe wall. This calculation was performed using Eq. (1) [27] which models fully developed flow of a fluid through a round pipe with constant wall temperature.

$$T_0 - T_s(x) = (T_0 - T_1)\exp\left[-\alpha * \frac{Nu}{r_0^2 * U} * (x - x_1)\right] \quad (1)$$

In Eq. (1), T_0 is the temperature of the fluid entering the heat exchanger, T_1 is the constant temperature of the heat exchanger's pipe wall, and T_s is the desired temperature of the fluid at the exchanger outlet. For the purposes of these experiments, no more than 50 degrees of superheat will be necessary. The temperature limits of the system and its components are a limiting factor in performing these experiments. 50 degrees of superheat in addition to the saturation temperature of steam at the highest desired pressure testing will bring us close to these temperature limits, therefore the left-hand side of the equation is equal to 50 degrees. If the temperature of the fluid leaving the heat exchanger can come within 2 degrees of the pipe wall this will be a satisfactory result, therefore $(T_0 - T_1)$ is equal to 2 degrees. The flowrate of the fluid through the cake, (U) has been measured experimentally. The pipe radius (r_0), gas thermal diffusivity (α), and kinematic viscosity (μ) are known. Solving Eq. (1) using these terms results in a distance $(x - x_1)$ of approximately 18 inches. The next size up after 18" is the 24" model. The 24" heat exchanger was chosen for purchase and will provide sufficient heat exchange surface and a factor of safety. Next, the electric heating source for the heat exchanger can be chosen.

The easiest electric heating source to be used for the heat exchanger is a flexible electric heating tape with a built-in thermostat. Various lengths, wattages, thicknesses, and voltages are available. Knowing the plate volume, density, and material specific heat, the heat transfer equation can be used to compare the required heating times of several heating tape options. All three of the

options would be capable of heating the heat exchanger to the required temperature but will vary in heating times. To perform the experiments in reasonable time frame it is desirable that the heating take no more than 10 minutes. Three potential options are listed in Table 4.

Table 4: Potential options for heating supply to the heat sink.

Option #	Thickness	Length	Wattage	Time required
1	0.5”	6 ft	216	17 min
2	1”	4 ft	144	25 min
3	1”	6 ft	432	8.5 min

Option 3 was determined to be the most practical to reduce wait times between experiments, and was purchased and installed with the heat exchanger.

Last, it would be helpful to perform a calculation to determine the maximum pressure experienced by the stainless-steel cylinder in a situation where the entrained cake solvent is evaporated instantly. The results of this calculation will determine the worst-case high-pressure scenario. If the resulting pressure is within the allowable range of the pressure cylinder, then there will not be any danger of the cylinder bursting during testing. This calculation is performed strictly as a safety concern. Assuming the vaporized solvent adheres to the ideal gas law, and knowing the amount of liquid solvent volume in a saturated filter cake, one can calculate the pressure inside the cylinder if that volume of entrained solvent were instantly vaporized. It was calculated that the highest possible pressure experienced by the pressure cylinder is 12 psig above the filtration/drying pressure. This is far below the allowable pressure of 200 psig for the cylinder. The possibility of the cylinder bursting due to rapid solvent evaporation is confirmed to not be a safety concern.

2.3.2 Experimental Apparatus Fabrication

After having performed all necessary calculations, the required materials to construct the steam system were purchased. An electric steam boiler (Sussman MBA series 3 kW model) is used to provide the steam. It can produce 9 lbs. per hour of saturated steam. It uses a 120-volt single-phase boiler feed pump and a pressure control system ranging from 0 to 100 psig. The electric heating source is a 480-volt 3 phase electric resistance heater, and the heat exchanger is ASME rated up to 100psig. The pressure regulating valve has a 3 to 25 psig setting range and a temperature rating up to 205°C. It is a McMaster-Carr #4674K63 cast iron model with 0.5-in. inlet and outlet. It has a bronze diaphragm with a PTFE seal and includes an internal strainer.

Downstream of the pressure regulating valve is a shutoff valve arrangement and a 4-pass high contact cold plate (AAVID Thermalloy). The plate is constructed of extruded aluminum with 9.5-mm. copper tubing. It is 5-in. wide by 12-in. long and 0.55-in. deep. The plate is preheated to the desired temperature and functions as a heat sink during the drying experiment. Its mass is large enough so that the gas temperature at its exit is maintained at the desired temperature setting during the short drying cycle. The gas temperature at the exit is within 2 °C of the plate itself. Hot system piping/hosing and the cold plate were wrapped in an electrical heat trace heating tape. The heating tape (model HSTAT101006, BriskHeat) has a thermostat control and provides electric heat as required to raise the temperature at the cold plate, and to maintain temperatures and prevent condensation in piping/hosing.

In addition to the above major components, Nickel-plated brass-bodied check valves with stainless steel springs were installed to protect the nitrogen and steam reservoirs. The check valves are 0.375-in. piston type. System piping includes both 0.5-in. type K copper and 0.5-in. cast iron.

All hot parts of the system except for the cylinder are insulated with 2-in. rigid fiberglass insulation with vinyl facing suitable for temperatures up to 230°C.

Omega type-K plug thermocouples were used to monitor temperature at various points in the system. They are suitable for temperatures up to 650°C and have a 6-foot cable insulated with fiberglass and covered with a stainless-steel sheath. Thermocouples are wired to a MadgeTech TCTempXLCD datalogger to record temperatures throughout the experiment. The datalogger has four channels, ranging from -270 to 1370°C for type K thermocouples, is accurate to within +-0.5°C, and can record temperatures every 0.1 seconds

Steam and nitrogen pressures in the cylinder are measured with an Ashcroft commercial pressure gauge suitable for steam, rated for use up to 100psig, and accurate to within +-3% of span.

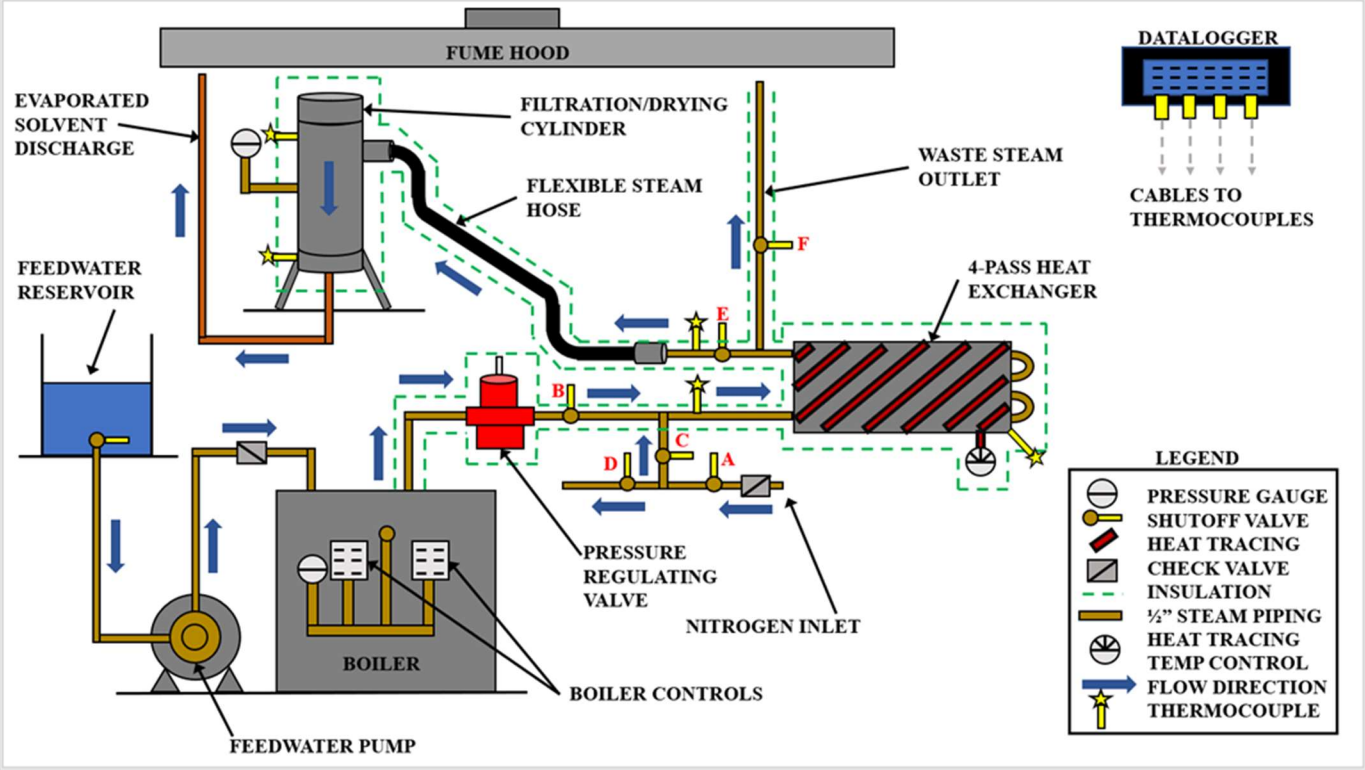

Figure 8: A fabrication design schematic of the modifications to the filtration equipment to accommodate nitrogen filtration, nitrogen drying, heated nitrogen drying, and superheated steam drying. This design will be used for preliminary system testing and may require changes during troubleshooting.

In Figure 8, the combined steam and nitrogen drying system is shown. Starting at middle left, feedwater is stored in the reservoir open to atmosphere. From here, water is pumped by the feedwater pump, through a check valve, and into the boiler. On the front of the boiler system there is a pressure gauge, pressure setting, and an overpressure setting. The water in the boiler is heated and changes phases to steam. The steam exits the top of the boiler and enters a pressure regulating valve. This valve is adjusted to set the desired steam delivery pressure for each experiment.

Downstream of the regulating valve is a shutoff valve that is open during steam operation and closed during nitrogen operation. Below this valve, there are three other valves that can be opened/closed depending on if the system is using heated nitrogen for drying, or room temperature nitrogen for filtration. Past this piping tee, there is a thermocouple. This is one of the five thermocouples in the system that are used to monitor temperature at various points. These thermocouples are wired into the datalogger to record temperature data versus time. Downstream of the first thermocouple is the plate-and-tube 4-pass heat exchanger. The heat exchanger is wrapped in an electrical heat trace heating tape. The heating tape has a thermostat control, and the temperature of the heat exchanger is also monitored by thermocouple.

After exiting the heat exchanger there is another tee with a shutoff valve in either direction. These valves can be opened/closed to allow the system to be used for drying, or for purging the system to a waste outlet directed into the hood. If the system is operating in a drying setting, the gas passes another thermocouple and then enters a flexible hose that is used to make a final connection to the cylinder. The cylinder itself also has two thermocouples to monitor temperature in different locations, as well as a pressure gauge. After the steam passes through the particle cake at the bottom of the cylinder, it exits through a plastic tube and is directed into the fume hood. All

the “hot” components of the system are insulated. The insulation is shown by the green dashed line. This is the system layout that was used for preliminary testing.

The next step was to fabricate the system as shown in the schematic. There are two steps in the fabrication that did require assistance from a mining department team member with electrical and plumbing experience. First, the 480v boiler needed to be wired and connected to high voltage power. Second, there are two connections at the heat exchanger plate that required soldering. A lead-free solder suitable for temperatures above 150 degrees C was chosen, and the piping was connected by the department helper. The rest of the fabrication consisted of connecting threaded pipes, installing insulation, and other things not requiring any professional help. System fabrication is shown in Figure 9, Figure 10, Figure 11, and Figure 12.

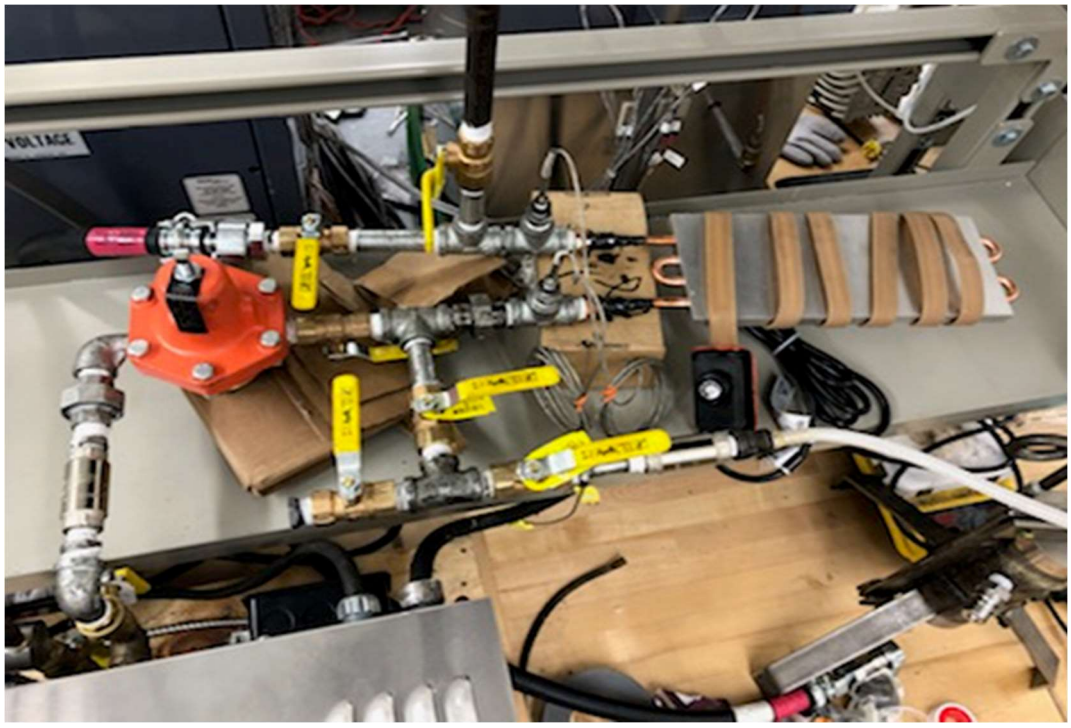

Figure 9: Piping components prior to being insulated. Piping is shown leaving the boiler and passing through the pressure regulating valve, shutoff valves, heat sink plate, and finally the flexible hose.

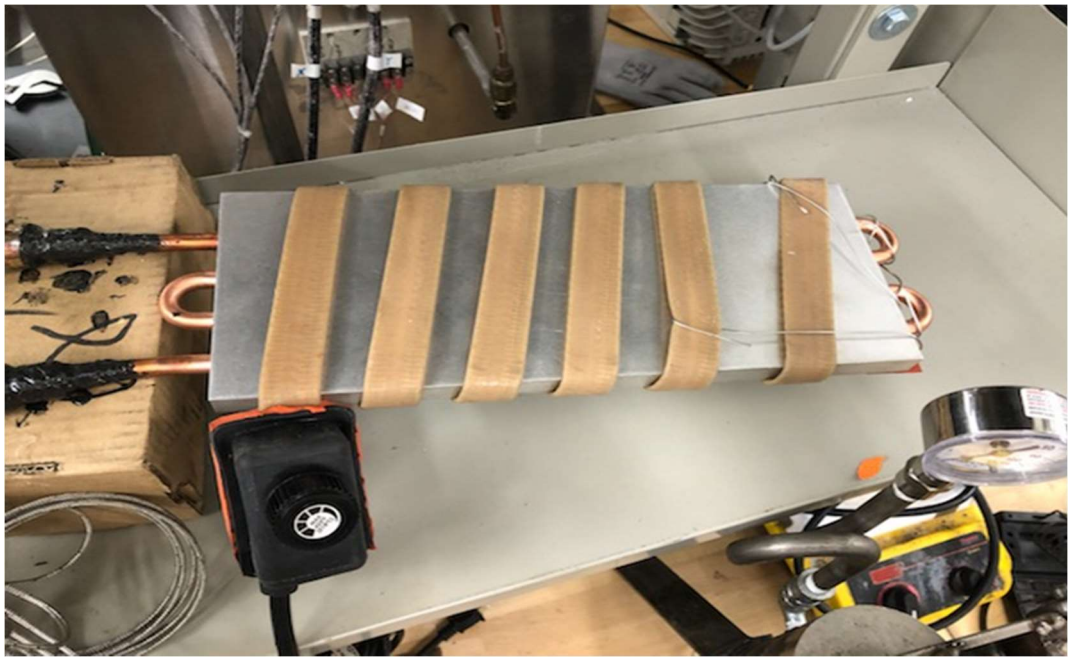

Figure 10: The heat exchanger plate is shown wrapped in electrical heating tape. The heating tape comes with an adjustable thermostat to set the steam or nitrogen temperature used for drying. A thermocouple will be attached to the plate to verify temperature settings.

Figure 11: The system is shown with the addition of the 2" thick high temperature fire resistant insulation.

Figure 12: The pressure filtration cylinder modified to accommodate the flexible steam hose for steam injection, and a steam pressure gauge to monitor drying pressure. Insulation was added after taking this photo.

With fabrication complete, the system was ready for preliminary testing. First, the system was pressurized with nitrogen. All the valves were closed, and the system was left overnight. The next day the pressure gauge was checked. The system was still under pressure at the same gauge pressure as the previous night, and it was confirmed there were no leaks. Next, nitrogen is passed through the system and each of the different gas flow settings were tested. When everything was verified to be operating correctly, the next step was to turn on the heat exchanger and run heated nitrogen through the system. When this was confirmed to operate successfully, the system was

tested with steam. After verifying that the steam is operating correctly, the first superheated steam drying tests began.

The preliminary superheated steam drying tests presented the first troubleshooting issues for the system. When steam was injected into the cylinder to dry a nitrogen formed particle cake, the cylinder became flooded with condensate in under 10 seconds. Testing was continued with higher steam pressure, and higher superheat temperatures. While this was able to slightly reduce the condensate formed in the cylinder, it still flooded and could not be reevaporated by the prolonged injection of superheated steam. At this point testing was stopped and it was necessary to develop a solution to the condensate issue.

2.3.3 Experimental Apparatus Troubleshooting and Modifications

During preliminary testing it had become apparent that the amount of condensate generated by the steam passing through the system and entering the cylinder was significant. There were three separate system components contributing to the formation of condensate. The piping immediately downstream of the boiler and continuing until the heat exchanger, the piping and flexible hose downstream of the heat exchanger, and the cylinder itself. Figure 13 shows a coal cake that was removed from the cylinder after an attempted steam drying experiment. The filter became flooded with condensate and began to leak water from the discharge. The cake itself could not begin to dry because it was saturated with water and the system overflowed before condensate could be re-evaporated. In order to successfully dry the coal cake using this system, the three problematic sources of condensate needed to be remedied.

Figure 13: A wet coal filter cake after being removed from the condensate flooded filter. The water on the wood surface around the cake was from steam condensing in the filter cylinder.

By adding an electrical heating tape to the piping and the flexible hose, the formation of condensate in these areas could be eliminated. The insulation was removed from the piping/hose, the heating tape was installed, and then the insulation was reapplied. With this addition to the system, the piping/hose heating tapes could be set at the saturation temperature of the steam used for drying.

Condensation forming in the cylinder itself was a more difficult problem to solve. The cylinder itself could not be wrapped in a heating tape and set to a high temperature for multiple reasons. If the cylinder temperature were raised before filtration, it would be dangerous to pour the cool solvents into the cylinder. If the cylinder temperature were raised after filtration, but before the initiation of steam drying, the heating tape itself would begin to dry out the cake and the experimental data generated would not be an accurate portrayal of the drying effect of the steam itself. The most feasible solution appeared to be adding an insulation layer to the inside of the cylinder to separate the steam from the stainless-steel cylinder wall. The diameter of the cylinder itself was only 2.5”, so the insulation layer would have to be thin to still allow formation of a cake with reasonable diameter.

The first option considered was an aerogel type of insulation. The cost to insulate the inside of the cylinder with aerogel was relatively cheap and it was easy to acquire. A square foot sheet of ¼" thick aerogel was less than $100. However, it presented challenges in that it would be difficult to affix it to the cylinder wall, and it was very porous and would become saturated with the steam drying medium. Different sealant or waterproofing methods of the aerogel insulation were researched, but most of these materials did not have the high temperature tolerance required for superheated steam.

A second option to consider was using a rigid insulation, such as a high temperature resistance, low thermal conductance plastic. PEEK (polyether ether ketone) met all these requirements. PEEK material is readily available from many suppliers and is machinable. The first step in acquiring the PEEK insulation tube was to perform calculations and a simulation of its insulating properties with the superheated steam used for the drying experiments. These calculations were performed using a finite element package COMSOL. The goal of this calculation was to determine the amount of condensate produced by the existing cylinder baseline model, and then to create a model with a selected PEEK insulating tube to verify that it will reduce condensate formation significantly.

The COMSOL Multiphysics software is a finite element solver used for many different applications including heat transfer. The software allows users to construct a physical model of a test system, develop a mesh, and then the heat conduction equation can be solved to simulate conduction through the system walls. First, a representative model of the steel pressure cylinder was constructed including the coal filtration cake. The dimensions of the cylinder itself as well as the cake were input into the software. Next, the heat capacity, density, and thermal conductivity of the steel and the coal cake were defined.

At t=0 the system will be at room temperature, 20°C. At t=0+ the inner surface of the cylinder is raised to 121.1°C, the saturation temperature of steam at 15 psig. The no heat flux boundary condition is prescribed on the outside of the cylinder. The constant temperature boundary condition on the cylinder's inner surface is imposed to mimic the fact that, due to the rapid condensation of steam on the surface, the temperature of the inner surface is pinned to the saturation temperature of the steam. The simulation is then run for 60 seconds. The software produces a plot of the temperature distribution of the clyinder. This calculation is then repeated several times with a similar model that has included a PEEK insulation tube until the PEEK dimensions have been optimized. The resulting temperature profiles are shown in Figure 14 and Figure 15 for the uninsulated cylinder, and the cylinder with the optimal 0.5" thick PEEK tube insulation respectively.

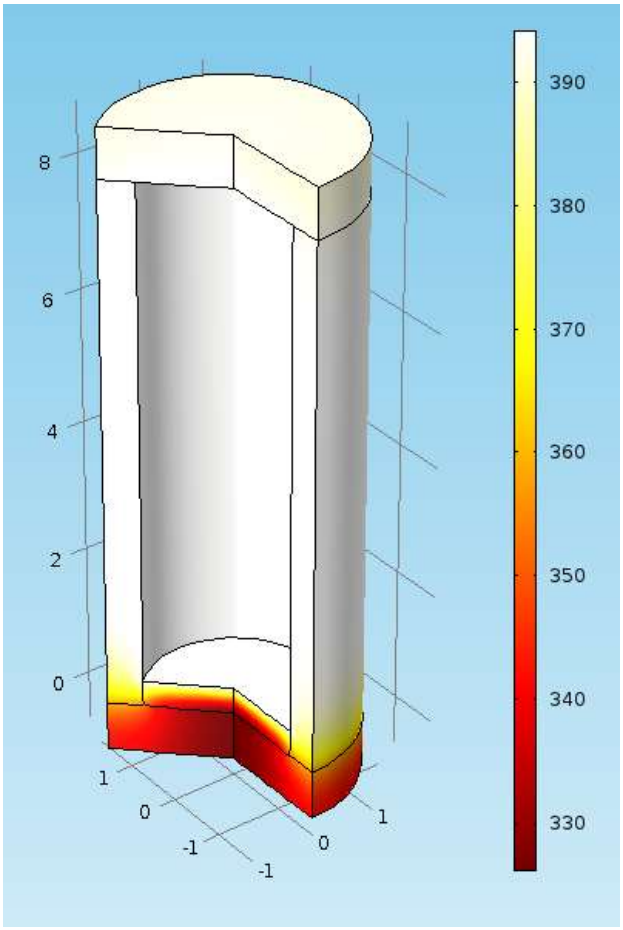

Figure 14: Temperature profile of the steel cylinder after injecting 15 psig steam for 60 seconds. The cylinder dimension scale is in inches, and the temperature color scale is in K. The saturation temperature of the 15 psig steam is 394K.

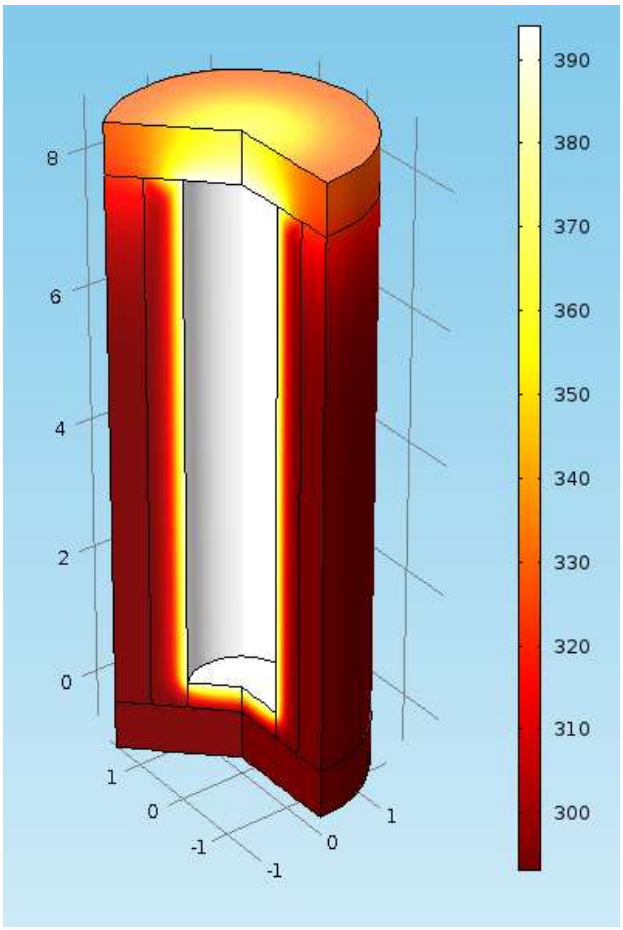

Figure 15: Temperature profile of the steel cylinder with PEEK insulation tube after injecting 15 psig steam for 60 seconds. The cylinder dimension scale is in inches, and the temperature color scale is in K. The saturation temperature of the 15 psig steam is 394K.

In Figure 14, after 60 seconds, nearly the entire cylinder except for the bottom cap portion below the coal cake has reached the saturation temperature of the steam. It is obvious that a significant amount of energy is wasted heating the cylinder steel, and forming condensate, rather than drying the coal cake. After the addition of the PEEK tube in Figure 15, the heat transfer through the cylinder side walls is substantially reduced. It is observed that only about half of the ½" thick PEEK tube experiences any temperature change at all. Most of the heat loss is through the cap at the top of the cylinder that has no PEEK insulation. The large majority of the steel remains near the 273K initial system temperature. While it is visually apparent that a 0.5" thick

PEEK tube will significantly reduce condensate formation, a more precise estimation can be calculated by integrating the temperature (and thus internal energy) change over the volume of the cylinder to obtain the heat heat transfer through the inner surface of the cylinder. Dividing this value by the volumetric latent heat of vaporization yields the volume of condensate formed for both models. Condensate formed vs time for both scenarios is plotted in Figure 16.

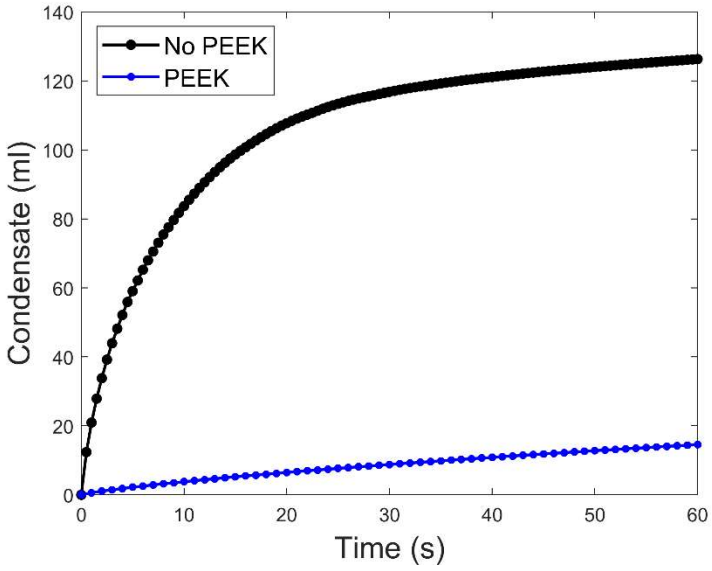

Figure 16: Condensation as a function of time for the steel cylinder with no PEEK insulation tube in black, and with the PEEK insulation tube installed in blue. The PEEK insulation reduces the volume of condensate formed inside the cylinder over the course of 60s from over 120ml to approximately 18ml.

Observing Figure 16 it is seen that the PEEK tube reduces condensate by nearly a factor of 7 at 60s. Additionally, because the condensate volume in non-insulated cylinder rises sharply, and that in PEEK-induced cylinder rises much shallower, condensate is reduced by close to a factor of 10 at the 15-20 second mark and thus is even more beneficial for experiments less than ~40 seconds.

Having determined that 0.5” is an acceptable PEEK wall thickness, the interior of the cylinder was measured with a micrometer to provide the sales company with a highly accurate

measurement so that the PEEK tube would fit into the cylinder properly. The supplier took a solid cylinder of the PEEK material, and machined it to the required inside and outside diameters. When the tube arrived at the lab, mining department machinists drilled the additional holes required for the steam and nitrogen supply, and the thermocouples. The installed tube is shown in Figure 17.

Figure 17: The pressure filtration cylinder with the PEEK insulation tube installed.

With the PEEK tube installed, and the additional heating tapes added to the system, preliminary testing was able to continue. Tests were run with 5, 10, and 15 psig steam superheated to 150 degrees C. The reduction in condensate was significant. There was no longer any flooding of the drying cylinder. The coal cake was much dryer upon inspection and crumbled when being removed from the cylinder. It formed a fine, dry powder when inspected visually. Moisture content was tested in the lab analyzer and was found to be below five percent. Figure 18 is a photo of a coal cake removed from the filter after steam drying with the newly installed PEEK tube.

Figure 18: A crumbled coal cake removed from the cylinder after steam drying. There was no condensate visually present on the cake when it was removed. The PEEK insulation tube appeared to solve the steam condensate problem.

There was also no visible condensate buildup on the particle cake itself, or on the walls of the cylinder. Whatever small amount of condensate did form during the drying experiment appears to have been reevaporated by the superheated steam. Unfortunately, before final testing could begin, another issue arose with the heat exchanger solder connections. The solder material had not been durable enough to withstand the electrical heating tape, and the high temperature super-heated steam. A small leak had formed at the heat exchanger and was preventing the system from maintaining pressure. Again, the system had to be disassembled and the solder was redone with a higher temperature resistant solder material. After this small fix, the system was running smoothly, and official testing and sample collection could begin.

Given the requirement for the filtration/drying system to perform several different functions, a valve control diagram was developed for five different gas flows. The system can utilize unheated nitrogen for filtration or drying, heated nitrogen for drying, steam for drying,

steam for purging the system, or nitrogen for purging the system. The gas flow valve settings are shown in Figure 19. Figure 20 is the modified schematic of the system after troubleshooting.

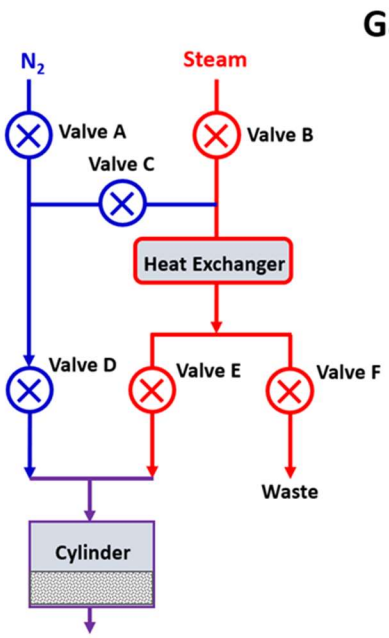

Flow Setting

1: Nitrogen filtration, unheated nitrogen drying
2: Nitrogen system purge
3: Nitrogen heated drying
4: Steam system purge
5: Steam superheated drying

Valve State (√=open, x=closed)

	A	B	C	D	E	F
1	√	×	×	√	×	×
2	√	×	√	×	×	√
3	√	×	√	×	√	×
4	×	√	×	×	×	√
5	×	√	×	×	√	×

Figure 19: A valve schedule detailing the different flow options provided by the filtration/drying system.

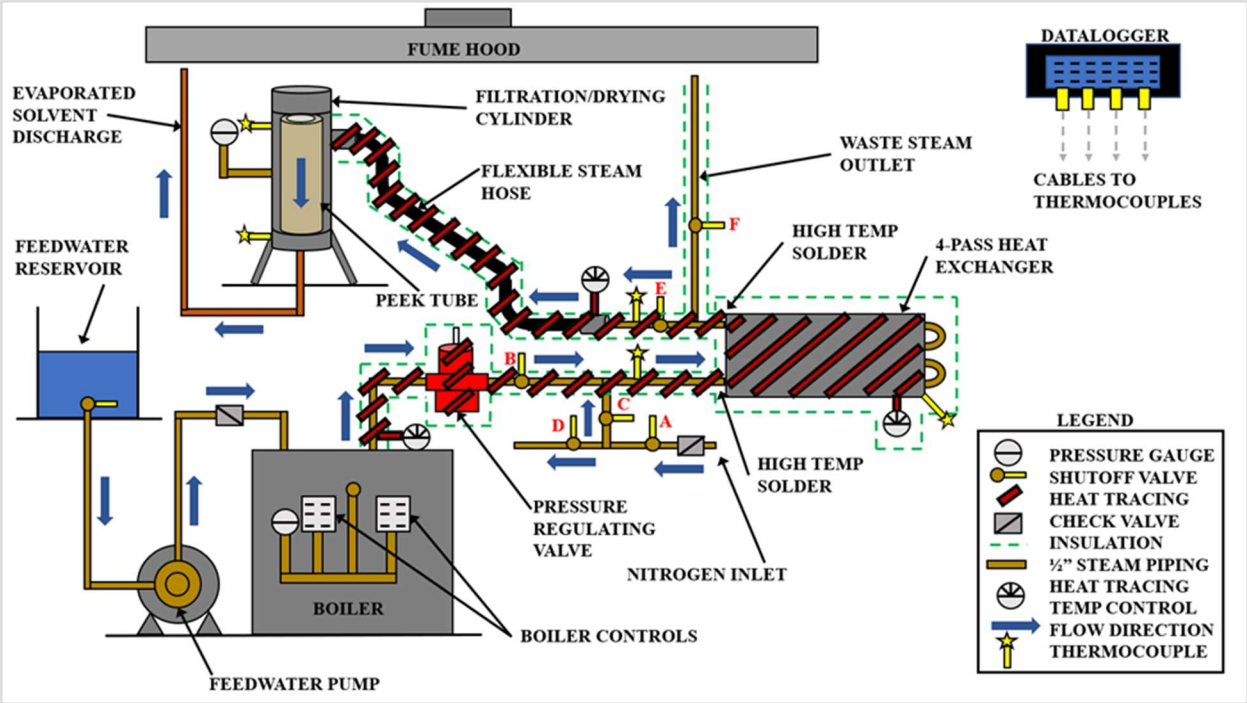

Figure 20: The final fabrication design of modifications to the filtration equipment to accommodate nitrogen filtration, nitrogen drying, heated nitrogen drying, and superheated steam drying. Electrical heating tape has been added to piping to prevent condensation, and high temp solders have been added to reinforce connections to the heat exchanger plate. The PEEK tube has been added to the pressure filter.

Before drying, filtration was completed by bypassing the filtration gas around any heated parts of the system. The filtration cake was left in the cylinder. To begin drying, all system temperatures were verified to be at the desired setting. Valves are then set to the desired flow setting, and the drying gas was injected into the cylinder until the desired time interval has been reached. During the drying process, the gas temperature is monitored and recorded to ensure consistent results. At the end of the drying process, the drying gas supply valve was closed, and the coal cake was removed from the cylinder. Samples of the coal cake were collected and stored for chromatography testing. The final experimental procedure is described below.

2.3.4 Experimental Procedure

1. Perform pre-start system checks;

2. Turn on heat exchanger electric heat tape;

3. Fill water feed reservoir to fill line on reservoir tank;

4. Open water feed reservoir shutoff valve;

5. Set steam generator, and pressure reducing valve to desired pressure;

6. Verify that nitrogen gas valve “C” is closed;

7. Verify that steam valve “E” is closed;

8. Verify that nitrogen gas valve “D” is open;

9. Verify that steam valve “F” is open;

10. Verify that steam valve “B” is open;

11. Turn on steam generator and feed pump;

12. Pour coal slurry sample into cylinder;

13. Turn on nitrogen tank and perform nitrogen pressure filtration;

14. Close nitrogen valve “A”;

15. Close nitrogen valve “D”;

16. Verify temperature at heat exchanger has reached desired setting;

17. Close steam valve “F”;

18. Open steam valve “E”;

19. Allow superheated steam to dry filter cake for desired team;

20. At completion of drying, turn off steam generator and pump;

21. Close steam valve “E”;

22. Close steam valve “B”;

23. Remove filter cake sample;

24. Break up and mix dry filter cake with spoon and collect several grams to be analyzed;

25. Store sample in sterile vial with stir tube and refrigerate;

26. Wait until cylinder returns to acceptable temperature level before pouring new slurry sample;

27. Repeat process from step “5” until testing is complete;

28. Begin shutdown procedure.

2.3.5 Experiments Performed

Table 5 summarizes the experimental parameters used in the drying tests. It is desirable to compare drying performance of nitrogen versus steam, while also identifying ideal temperature and pressure operating conditions. Pentane and Hexane at room temperature are used to provide a baseline result before adding heating. Solvent vaporization testing was performed using filtration cakes from 10% by weight solvent-coal slurries.

Table 5: Experimental Parameters for the vaporization stage of the two-step solvent removal process.

Test number	Drying gas	Solvent type	Drying gas pressure (psig)	Drying gas temperature (°C)	Drying time intervals (s)	Cake formation method
1	Nitrogen	Pentane	20	20	30, 45, 60, 75, 90, 105, 120	pressure filtration using 20psig N_2
2	Nitrogen	Hexane	20	20	60, 120, 180, 240, 300	pressure filtration using 20psig N_2
3	Nitrogen	Hexane	20	100	60, 120, 180, 240	pressure filtration using 20psig N_2
4	Nitrogen	Hexane	20	150	60, 120, 180	pressure filtration using 20psig N_2
5	Nitrogen	Hexane	30	150	60, 120, 180, 240	pressure filtration using 20psig N_2
6	Steam	Hexane	5	150	20, 35, 65	pressure filtration using 20psig N_2
7	Steam	Hexane	10	150	15, 30, 60	pressure filtration using 20psig N_2
8	Steam	Hexane	15	150	5, 10, 15	pressure filtration using 20psig N_2
9	Steam	Hexane	5	180	20, 35, 65	pressure filtration using 20psig N_2
10	Steam	Hexane	15	150	3, 6, 9, 15	Vacuum filtration

2.4 Chromatography Analysis

In typical drying experiments, drying is monitored by continuously measuring the mass of the sample being dried. This is because the sample is often isolated from the housing of the drying vessel, and low operating pressure was involved. In the process studied here, continuous monitoring of the drying is challenging to implement. The amount of solvent in the filtration cake to be vaporized and removed is extremely small (typically less than a gram), and the final residual

solvent must be reduced to tens of milligrams. The drying vessel (the pressure cylinder), however, weighs more than 5 kg. Therefore, a highly sensitive measurement of the solvent content of the cake must be conducted, and building a continuous solvent content measurement system is beyond the resources available to us. Therefore, many tests were performed with different drying times. Samples of filtration cakes obtained at the end of these tests were analyzed using gas chromatography to determine the solvent concentration in them. This reduced the time resolution of the drying curve, but accurate drying data are available at pre-selected drying time, and the overall drying trends are still apparent.

After each drying experiment, the coal cake was removed from the cylinder and broken apart. 3 to 4 grams of the coal sample were placed into a sterile vial and refrigerated. Later, the samples were delivered to the chemistry chromatography lab for testing. Solvent concentration results are returned as parts per million (ppm) value.

All organic solvents (Hexane and pentane) and SPME fibers were obtained from Sigma-Aldrich (St. Louis, MO) and used as received. All standards were prepared by direct transfer of 0.6, 1, 2, 3 and 4 μL of hexane or pentane to a 5 x 40 mL of screw-top, septum-sealed headspace vial containing a magnetic stir bar. Next, each vial was heated using a water jacket at 56°C for 10 minutes and stirring to obtain equilibrium. Then, an SPME fiber (Divinylbenzene/Carboxen/Polydimethylsiloxane, 50/30μm DVB/CAR/PDMS, 24 ga, 1cm length for manual injection) was placed inside the 40 mL vial and 5 minutes sampling was obtained. Finally, SPME fiber was injected onto the GC/FID and quantitative results were obtained.

For quantitative analysis, each sample was prepared by direct weighing a known mass of sample in a 40 mL of screw-top, septum-sealed headspace vial containing a magnetic stir bar. Each

sample was heated using a water jacket at 56°C for 10 minutes and stirring to obtain equilibrium. Next, an SPME fiber (Divinylbenzene/Carboxen/Polydimethylsiloxane, 50/30µm DVB/CAR/PDMS, 24 ga, 1cm length for manual injection) was placed inside the vial and 5 minutes sampling was obtained. Next, the sample was injected onto the GC/FID for the quantitative analysis. All GC/FID analyses were performed using Agilent (Wilmington, DE) 6850 GC equipped with flame ionization detector (FID). Separations were obtained using an HP-1 capillary column (30 m long x 320 µm I.D. with a film thickness of 0.25 µm) from Agilent. Operating parameters for gas chromatography analysis are shown in Table 6.

Table 6: GC operating parameters.

Injection Port Temperature	280°C
Purge Valve	3 mL/min
Purge Time	1 min
Total Flow	33 mL/min
Constant Flow	1.5 mL/min
Injection	Manual, split 1:30
Column Oven Initial Temperature	40°C
Column Oven Initial Time	3 min
Column Oven Ramp Rate	35°C/min to 250°C
Column Oven Final Temperature	250°C
Column Oven Final Time	1 min

Chapter 3. Results

This section presents the results of in-situ solvent recovery that combines filtration and solvent vaporization. Results on liquid-solid separation through filtration are presented first, followed by solvent removal from the filtration cake through vaporization and convection by a carrier gas. As mentioned earlier, to be viable for integration with the HHS-based coal dewatering technology, the filtration and drying steps must be completed in 60 seconds and 10 seconds, respectively. This is to ensure that the process can effectively be scaled up to the pilot or commercial stage using readily available filtration and drying equipment. In addition, the mass loading of residual solvents in the filtration cake at the end of the drying step should be below 1,400 ppm.

3.1. Liquid-solid separation through pressure filtration

The first experiments conducted were filtration kinetics tests using various coal slurries. These tests allowed an appropriate percent solid and filtration pressure to be chosen for the subsequent drying experiments. Figure 21a and b present the filtration curves for pentane-coal slurries with 10% and 15% solid mass loading, respectively. The filtration curves show several common features. First, the liquid mass collected has an initial value above zero at $t = 0$ (see, e.g., the curve at 60psig in Figure 21a). Next, though not obvious in all cases, the filtrate mass increases nonlinearly with time before reaching a peak value. Finally, the mass collected decreases very slightly at large time.

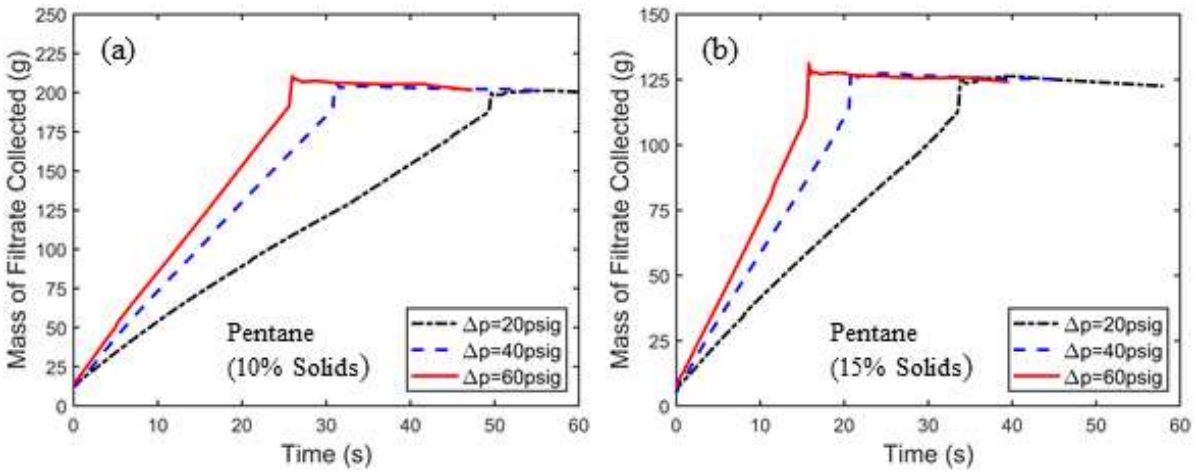

Figure 21: Mass of filtrate collected vs. time during filtration of pentane-coal slurries with a solid mass loading of 10% (a) and 15% (b) under a filtration pressure drop of 20,40, and 60 psig.

The initial mass collected is due to a small portion of solvents passing through the filter via gravity after the slurry was poured into the vessel, but before the filtration pressure was applied. The nonlinear filtrate mass curve is caused by the three stages of a filtration process as elucidated by Huang et al (2018) [10]. Specifically, a filtration process involves three stages. Taking the filtration at 60 psig and 10% solid mass as an example (see Figure 21a), in the first stage, which ends at $t\sim$ 10s, the filtration rate decreases as the filter cloth/paper beneath the slurry (referred to as filter medium hereafter) becomes increasingly clogged. In the second stage, second region, from 10 to 25 s approximately, the filtration rate decreases further. During this stage, more and more coal particles collect on the filter paper and the filtration cake forms and becomes thicker. Liquid solvents flow through the capillaries formed between coal particles. Since the length of the capillaries, and thus the flow resistance, increases with time, the filtration rate decreases with time.

In the first and second stages, the filtration is governed by the liquid-solid two-phase flow in the filtration cake. In the final stage, which begins at ~26 s where a sharp upwards jump of filtrate mass is seen, the filtration is dominated by gas-liquid-solid three-phase flows: the beginning of the jump in filtrate mass is when the filtration gas begins to penetrate the filtration cake, and marks

the transition from two- and three-phase flow in the filtration cake. The abrupt end of the jump is when the filtration gas exits the filtration cake. The jump in filtrate mass is also caused partly by the impact of the last remaining film of solvent liquids being forced out of the filtration cake on to the filtrate collection vial that sits on the mass balance.

The time at which the abrupt end of the jump in filtrate mass is taken as the filtration time t_f. At $t = t_f$, the third stage of the filtration process finishes, and in-situ evaporation and removal of solvent vapor by filtration gas (here, N_2) start. Clearly, the filtration time is dominated by the first and second filtration stages. Figure 21a shows that the filtrate mass decreases slightly from 27 s to 50 s. This decrease is due to the vaporization of the highly volatile pentane collected in the filtrate collection vial.

From the data shown in Figure 21, filtration times for different slurries and filtration pressure are obtained. Figure 22 shows that, at the same filtration pressure, the filtration times for slurries with a 15% solid loading is about 10-15% shorter than with a 10% solid loading. This is caused by the smaller amount of solvent in the latter slurries. Figure 22 also shows that, as the filtration pressure increases, filtration time decreases nonlinearly, e.g., the reduction of filtration time as filtration pressure increases from 40 to 60 psig is ~40% of that which occurs when the filtration pressure increases from 20 to 40 psig. The nonlinear dependence of filtration time on filtration pressure is attributed to the different filtration cake structure under different filtration pressure.

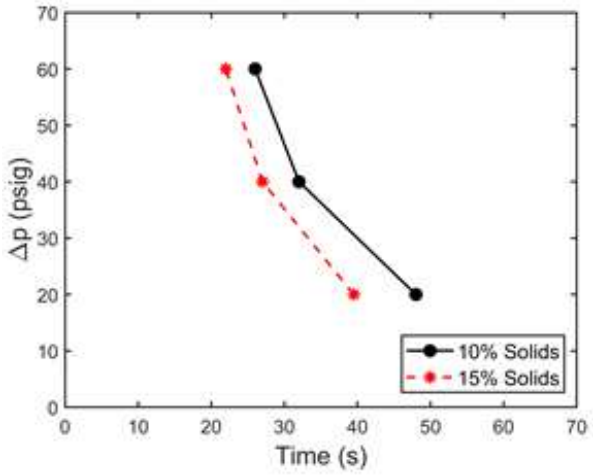

Figure 22: Dependence of the filtration time on filtration pressure (Δp) for pentane-coal slurries with 10% and 15% solid loading.

As noted earlier, the filtration time is controlled primarily by the duration of the first and second stages of a filtration process. As filtration pressure increases, the filter medium becomes more highly clogged at an earlier time, which tends to prolong the first filtration stage. Furthermore, as filtration pressure increases, the filtration cake formed during the second filtration stage becomes more compact, resulting in decreased radii of capillaries between coal particles and thus increased flow resistance through the filtration cake [10]. Therefore, even though higher filtration pressure provides a larger driving force for solvents to flow through the filter medium and develop a filtration cake, it also elevates the resistance for solvent flow through them. Consequently, as filtration pressure increases, filtration time does not decrease linearly. In practice, the filtration pressure may be optimized by balancing energy consumption and throughput, which is out of the scope of the present work.

Next, filtration tests were conducted for hexane-coal slurries. Figure 23 shows the filtration kinetics for slurries with 10% and 15% mass loading of coal at three different filtration pressures. The shape of the filtration curves is qualitatively similar to those shown in Figure 21. A notable difference is that, after the third filtration stage when the N_2 gas breaks through the filtration cake,

the filtrate mass collected shows no noticeable decrease. This is expected because hexane is much less volatile than pentane and mass loss due to evaporation is suppressed for hexane. Figure 24 presents the filtration time for hexane-coal slurries with 10% and 15% solid loadings at pressure differences of 20, 40, and 60 psig. A nonlinear dependence of filtration time on filtration pressure is again observed. Compared with the filtration time for pentane-coal slurries (see Figure 22), for the same filtration pressure, the filtration time for hexane-coal slurries is considerably longer. The longer filtration time is consistent with the fact that hexane has a viscosity 15% higher than pentane.

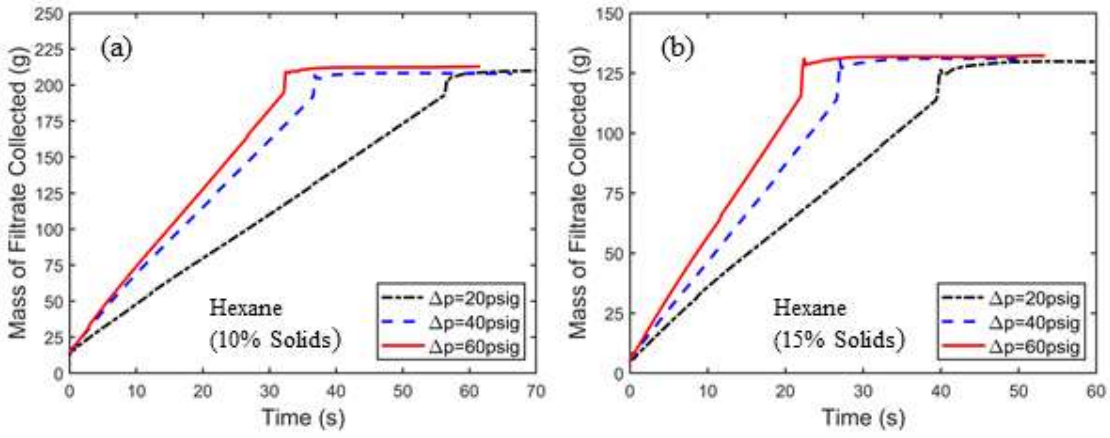

Figure 23: Mass of filtrate collected vs. time during filtration of hexane-coal slurries with a solid mass loading of 10% (a) and 15% (b) under a filtration pressure drop of 20,40, and 60psig.

Figure 22 and Figure 24 show that filtration can be completed within 60 s for pentane-coal and hexane-coal slurries with solid loading of 10% and 15%, even at the lowest filtration pressure studied (20 psig). Although the filtration time is slightly shorter for pentane, the more volatile pentane is more dangerous to handle than hexane and thus hexane is preferred in practical applications.

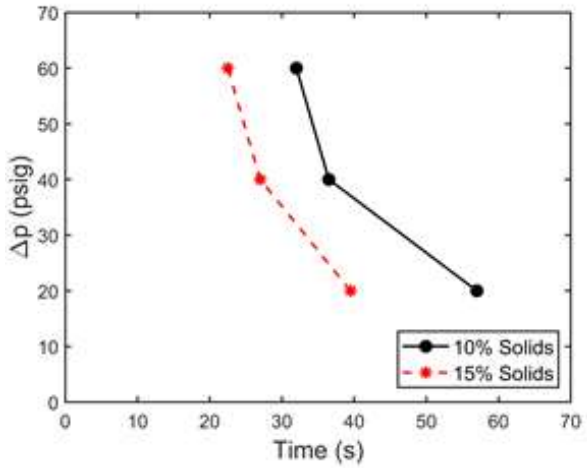

Figure 24: Dependence of the filtration time on filtration pressure (Δp) for hexane-coal slurries with 10% and 15% solid loading.

Having completed filtration testing, it is useful to characterize the filtration cake, whose structure can greatly affect the subsequent drying step. Such characterization, however, is very challenging. Because of the small size of coal particles, the size of pores within the filtration cake are small. Quantifying the size of these pores and their connectivity is difficult, not only because the filtration cakes are relatively delicate, but also because they are partially saturated by relatively volatile solvents. To overcome these difficulties, the approach developed by Huang et al (2018) is utilized [10]. In this approach, the filtration kinetics curves (e.g., those shown in Figure 21) are fitted to a model to extract the effective radius of the capillaries in the filtration cake. The model was derived from first-principles using the Navier-Stokes equation under the assumption that the filter cake consisted of a bundle of well-defined capillaries of identical radius. The model considered the two- and three-phase flows through a filter cake during the cake formation. Eq. (2) shows that the model for two-phase flow during cake formation:

$$Q = \frac{dV}{dt} = \frac{A^2 \Delta P}{\mu \left[\frac{8 X_S V}{k R^2 \rho_s (1-k)} + A R_m \right]} \qquad (2)$$

This model relates the filtration rate Q (*i.e.*, volume of filtrate removed per unit time, dV/dt) to the filtration conditions including pressure difference (ΔP), solids content in the feed slurry (X_s), cross sectional area of the filter cake (A), particle density (ρ_s), solvent viscosity (μ), cake surface porosity (k), pore (capillary) radius (R), and resistance of filter medium (R_m).

An integral of Eq. (2) gives the volume of filtrate (V) for a given filtration time (t). Note here that the filtrate volumes measured as a function of time (V *vs.* t) as well as ΔP, X_s, A, ρ_s, μ, and k can be readily obtained from each filtration test. Therefore, one can determine the other model parameters, such as pore radius (R), and filter medium resistance (R_m) by fitting V *vs.* t curves calculated by integrating Eq. (2) to those obtained from filtration tests.

In the case of the pentane-coal slurry filtration shown above, (ΔP) varied between 20,40, and 60psig. (X_s), the % solids, was either 10% or 15%. The cake area (A) was $3.17 \times 10^{-3} m^2$. (ρ_s) for the coal sample used in all experiments was 1,400 kg/m^3. The viscosity (μ) of pentane at 20°C is 0.250 mpa·s. Cake porosity (k), a function of particle size, was estimated as 0.35. Finally, capillary (pore) radius (R) and medium resistance (R_m) are determined from fitting the model to the experimental curve.

Figure 25 displays the results of the curve fitting for the 10% solids in the 20 psig pentane filtration experiment, and quality of the fitting is good considering the complexity of the filtration process and the simplicity of the model. The curve fitting leads to a capillary radius of 1.28 μm in the filtration cake. This small radius is consistent with the small size of coal and will be used later in this paper to provide more insight into the drying behavior of the fine coal particle cake.

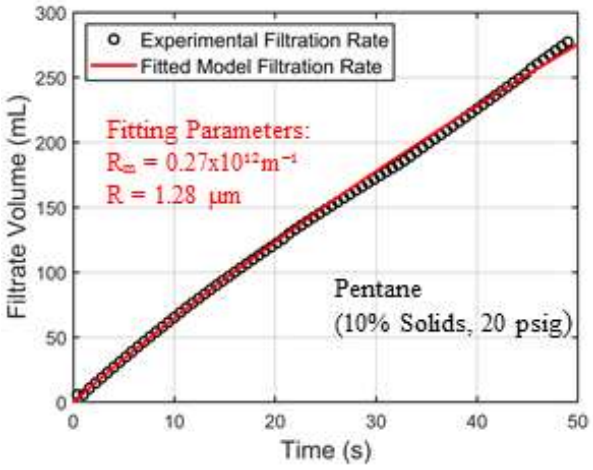

Figure 25: Experimental filtration results for the 10% solids pentane slurry at 20 psig (every third data point denoted by black circle) are fitted to the curve produced by the Huang et al (2018) model (red curve). The fitting parameters (R) and (R_m) resulted in a capillary radius of 1.28 μm, and a medium resistance of $0.27x10^{12}m^{-1}$.

Finally, it is useful to identify preferred filtration conditions from results in this section. The solid loading in slurries in the HHS process can vary between 10% and 15%. Given that filtration is slower with a 10% solid loading than 15% solid loading, it is beneficial to focus on slurries with an initial 10% solid loading so that the worst-case scenario is studied. Further, because the 20 psig tests were completed in less than 60 seconds, there is no need to use higher filtration pressures during drying testing.

3.2 Drying through solvent vaporization and convection

3.2.1 Room-temperature N_2 drying

Drying tests were conducted with room-temperature nitrogen as the carrier gas to obtain a baseline drying performance. In addition to drying filtration cakes obtained by filtration of hexane-coal slurries, drying of filtration cakes with residual pentane was also tested to serve as a reference for comparison. Figure 26 presents the drying curves for filtration cakes with pentane and hexane as a function of time. The pressure difference driving the nitrogen flow through the cake is 20 psig.

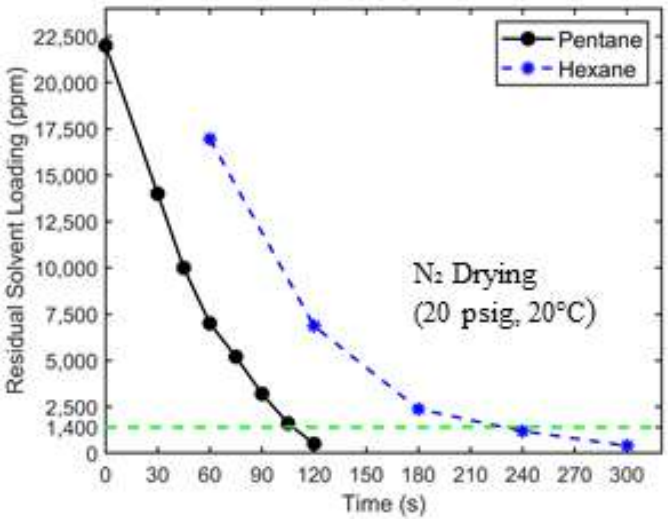

Figure 26: The drying curve of filtration cakes with pentane and hexane as residual solvents. 20 psig nitrogen at 20°C is used as the carrier gas. The target concentration of 1,400 ppm is denoted by a horizontal dashed line. The initial hexane loading is 24,500 ± 250 ppm.

Figure 26 shows that pentane is removed more quickly from filtration cakes than hexane. The residual pentane in filtration cakes reaches the target concentration of 1,400 ppm at ~105 s, while it takes ~230 s for hexane. To understand these results, it is noted that the drying of filtration cakes involves physical processes including phase charge, heat transfer, and mass transfer by diffusion and convection. The last two processes greatly affect the drying rate, and they depend strongly on the distribution of liquid solvents in filtration cakes. Establishing such distribution in a filtration cake by imaging is difficult because of the small pore size and low liquid saturation in the cake. The drying data in Figure 26, however, can help provide insights into the liquid distribution in filtration cakes. As mentioned earlier, there exist two limiting scenarios for the distribution of residual liquid solvent in a filtration cake. In the first scenario (see Figure 1a), at the end of the liquid-solid filtration step, liquid solvents form a continuous film transversing the filtration cake and are in close contact with the pathways of the carrier gas flow. In the second scenario (see Figure 1b), liquid solvents are trapped in tiny pores sparsely distributed in the filtration cake. Here, each major pathway of the carrier gas flow is in contact with a few liquid solvent clusters. To

examine which of these scenarios is closer to the actual scenario, analysis is performed for the drying time based on the first scenario. Without losing generality, our analysis focuses on the drying of filtration cake with pentane as residual solvents.

Figure 27a shows a pore-scale model of the drying process based on the first scenario, where a representative pore inside the filtration cake is initially covered by a thin film of residual solvents. Since our measurements indicated that the temperature of a typical filtration cake decreases less than 6°C during the entire drying process, the drying is approximated as an isothermal process. Furthermore, the slow drying shown in Figure 26 is not limited by the kinetics of evaporation at liquid-vapor interfaces. Instead, drying is governed by the diffusion of solvent vapor from the evaporation site (pore walls) to the interior of the pore and the carrier gas flow along the pore. Because of the pore's small radius R and its large length-to-radius ratio (L/R ~ 10^4), the gas flow in the pore is laminar and fully developed. Hence, the solvent removal rate from the pore can be estimated using the classical model for fully developed flows and mass convection in round pipes [27].

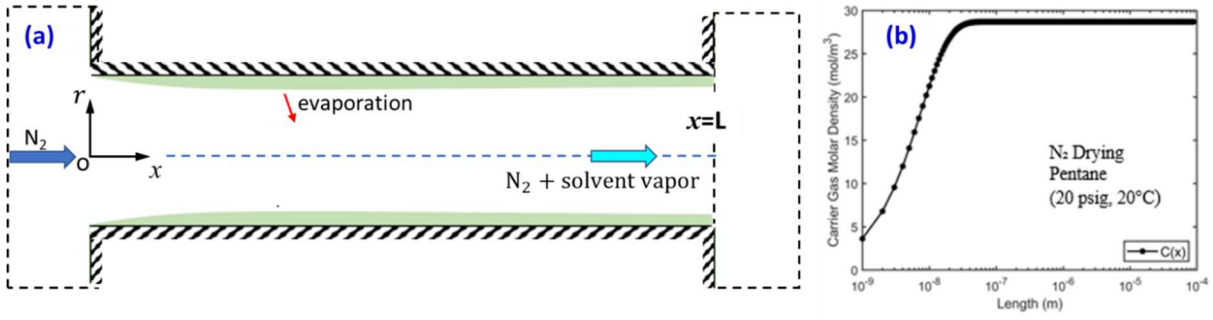

Figure 27: (**a**) A schematic of a pore-scale model for the drying (solvent vaporization and mass convection) of a filtration cake based on the assumption that the residual solvents form a continuous film on the pore walls. (**b**) Variation of the solvent vapor density along a representative pore (radius R = 1.28 μm; length L = 0.01 m).

Specifically, the average gas velocity in the pore is given by the Hagen-Poiseuille equation:

$$\overline{U} = \frac{\Delta P R^2}{8\mu L} \tag{3}$$

where ΔP is the pressure difference along the pore and μ is the viscosity of N_2. With the pressure difference (20 psig), pore length (0.01 m), and pore radius (1.28 μm) in our drying experiment, $\overline{U}$ is estimated to be 0.159 m/s. The density of solvent vapor on pore's surface is equal to the saturation density of the solvent, C_S, which is defined by the solvent temperature (here, 20°C). The density of solvent vapor along the pore is given by

$$C(x) = C_S - (C_S - C(0))\exp\left[-\frac{D_s Sh}{R^2 \overline{U}} x\right] \tag{4}$$

where $C(0) = 0$ is the vapor density at the pore's entrance, $Sh = 3.66$ is the Sherwood number, and $D_s = 8.85 \times 10^{-6}$ m^2/s is the diffusion coefficient of pentane in nitrogen. Using the average velocity computed above, the vapor density along the pore is obtained (see Figure 27b). It is observed that vapor density approaches the saturation density at a distance of $L/10^4$ from the pore's entrance. This short distance is consistent with the small characteristic length for vapor density to reach saturation, i.e., $L_s = R^2\overline{U}/D_s Sh$ (see Eq. 3). Physically, because of the small pore radius, the diffusion of solvent vapor from the liquid film on pore walls to a pore's center is facile. Meanwhile, the gas flow carrying the vaporized solvent downstream is slow. Hence, the carrier gas easily becomes saturated as it flows down the pore, and the vapor density at the pore's exit is always at the saturation density C_s.

Using the fact that the vapor density at the pore's exit is C_s and assuming that the filtration cake features bundles of parallel pores with the same radius R, an order of magnitude estimation of the time for the complete removal of solvent from a filtration cake can be obtained as

$$t_{dry} = \frac{8}{\pi}\frac{\bar{R}T}{p_s M_s}\frac{L}{\Delta p}\frac{m_{s,c}}{R_c^2 R^2}\frac{\mu}{k} \tag{5}$$

where $\bar{R}$ is the universal gas constant, T is temperature, p_s is the saturation pressure of solvent, M_s is the molecular mass of solvent, $m_{s,c}$ is the initial liquid solvent mass inside the filtration cake, R_c is filtration cake's radius, and k is filtration cake's porosity. Using the properties of filtration cake (R_c = 0.032 m, L=0.01 m, R = 1.28 μm, k = 0.35, $m_{s,c}$ = 0.563 g) and pentane (M_s= 72.15 g/mol and p_s =57.3 kPa), t_{dry} is found to be 1.88 s.

The drying time estimated above is almost 100 times smaller than that observed experimentally (120 s, see Figure 26). Such a dramatic discrepancy suggests that the basic assumption underlying the above estimation, i.e., the residual liquid solvents form continuous films lining the walls of the pathway of carrier gas flowing through the filtration cake, is inaccurate. Therefore, the second scenario for the distribution of residual solvent in the filtration cake is more likely, i.e., solvents exist as isolated liquid clusters sparsely distributed in filtration cakes, is more reasonable. The carrier gas is thus only in contact with "patches" of liquid solvents whose surface area is far smaller than the surface area in contact with the carrier gas flow. The remaining solvents are trapped in microcapillaries perpendicular to the main carrier gas pathway (see Figure 1b). Under this scenario, the carrier gas flow will not be saturated with solvent vapor when it leaves the filtration cake and thus the solvent removal is mainly limited by the transport of vaporized solvent from the evaporation site to the carrier gas flow pathway rather than by the convection of solvent vapor by the carrier gas flow.

The above analysis helps understand the drying curves in Figure 26. For example, the drying curves show that the drying rate decreases as solvents are removed from filtration cakes. Similar falling drying rate has been reported in many studies of the drying process in porous media, where the carrier gas usually flows over a porous media's surface [13, 28-30]. In those works, drying rate falls as the liquid saturation in a porous media becomes low. Under that condition, the capillary

flow of water and diffusion of water vapor to the porous media's surface become difficult, which slows down transport of water to the surface of porous media and hence the drying rate.

In the present study, although the carrier gas flows *through* filtration cakes, the distribution of the liquid solvent inferred from our above analysis is qualitatively similar to those revealed in previous drying studies. As such, similar falling drying rate can be expected. Figure 26 also shows that the drying of hexane is slower than pentane. This can be understood as follows. Here, the drying process is limited by the transport of solvent toward the pathway of the carrier gas flow. Because hexane has a lower vapor pressure than pentane, the flux of hexane from the evaporation site (solvent patch in contact with the carrier gas flow or solvents that have receded into micro capillaries connecting to the gas flow pathways) to the carrier gas flow pathway tends to be smaller than that of pentane. Consequently, the drying of filtration cakes with hexane is slower than that of pentane-loaded filtration cakes.

Overall, Figure 26 shows that the hexane and pentane content in a filtration cake can be reduced to the target level (1400 ppm) using room-temperature nitrogen flow. However, the cutoff drying times, defined as the time when the solvent content is reduced to the target level, are ~10-20 times longer than the 10 s interval needed by commercial deployment of HHS-based dewatering technologies. To reduce the cutoff drying time, one possible strategy is to increase the temperature of the carrier gas flow. This will increase the vapor pressure of solvent and facilitates the transport of solvent vapor to the carrier gas pathway within filtration cakes, thereby accelerating drying.

3.2.2 Drying using heated N_2

Having shown that room-temperature nitrogen cannot dry filtration cakes to the desired level within the required time, heated nitrogen with a pressure of 20 psig is used to dry cakes

obtained from pressure filtration of hexane-coal slurries with 10% solid loading. Figure 28 displays the drying curves when the nitrogen temperature is 20°C, 100°C, and 150°C. The results in Figure 28 exhibit several interesting features. First, there was a significant reduction in drying time when N_2 temperature is increased from 20°C to 100°C. With 100°C N_2, the hexane concentration in filtration cakes reaches the target concentration at ~150 s, 60-70 s shorter than when 20°C N_2 is used. Second, as N_2 temperature increases to 150°C, the improvement of drying performance is negligible. Finally, at elevated temperatures, the drying rate also decreases with time.

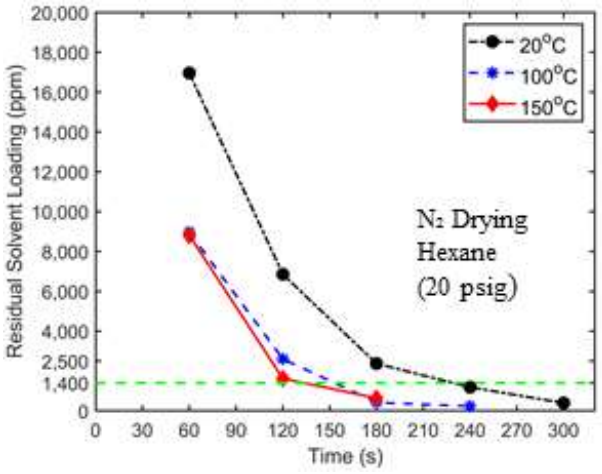

Figure 28: Hexane drying curves using 20 psig nitrogen at a temperature of 20°C, 100°C, and 150°C as the carrier gas. The target solvent concentration of 1,400 ppm is denoted by a dashed horizontal line. The initial hexane loading is 24,500 ± 250 ppm.

The reduction in drying time as N_2 temperature is increased from 20°C to 100°C is attributed to the fact that when the heated N_2 enters the filtration cake, it raises the temperature of the filtration cake and the liquid solvents in the cake. The latter increases the solvent vapor density in the cake, thereby facilitating more rapid solvent removal through mass convection. When the temperature of N_2 is elevated to 150°C, the cutoff drying time is shortened only marginally. It is interesting to note that hexane's boiling points are 69.0°C and 98.6°C at 0 and 20 psig, respectively. It thus appears that raising the carrier gas temperature to 100°C likely causes rapid vaporization of liquid

solvent that is absent when the temperature is 20°C. Further temperature rise above 100°C had less of an impact on the phase change of the liquid hexane. In the future, it would be interesting to perform experiments to examine how drying behavior varies as temperature increases from 69.0°C to 100°C.

The fact that the drying rate still falls after the solvent concentration inside the filtration cake falls to a low value (here, around 2000 ppm) even when the carrier gas temperature is increased above hexane's boiling point suggests that mass transfer from the evaporation site to carrier gas pathways remains a limiting factor in drying. The latter implies that violent phase change such as boiling, which should perturb coal particles in filtration cake to release trapped solvents and diminish the resistance for solvent transport to carrier gas flow through filtration cakes, does not occur at the temperature investigated here. The absence of boiling is likely caused by the fact that, for liquids trapped in sub-micrometer cavities, boiling is suppressed; instead, liquids become superheated, and phase change occurs only at their interfaces with solvent vapor or carrier gas.

Having seen little benefit to drying by raising N_2 temperature to 150°C, the next set of experiments will determine what effect is produced by increasing the pressure difference driving N_2 flow through the filtration cake. Figure 29 compares the drying curves when 150°C N_2 flows through the filtration cake at 20 and 30 psig pressure differences. It is observed that increasing the pressure of the carrier gas entering the filtration cake from 20 to 30psig resulted in a reduction in the cutoff drying time of ~30 seconds.

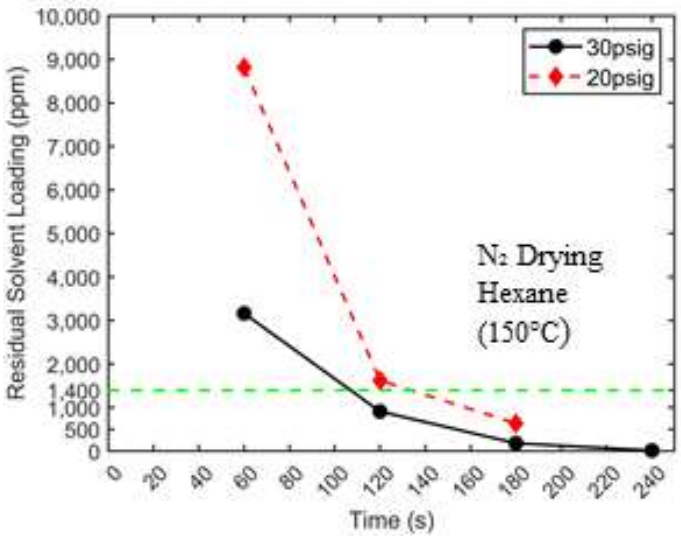

Figure 29: Hexane drying curves using 20 psig nitrogen at 150°C and 30 psig nitrogen at 150°C. The target solvent concentration of 1,400 ppm is denoted by a dashed horizontal line. The initial hexane loading is 24,500 ± 250 ppm.

The enhanced drying accompanying the increase of carrier gas pressure difference may be due to several factors. First, the higher N_2 pressure increases the density (and thus mass flowrate) of N_2 carrier gas entering the filtration cake. Therefore, the heat supplied by N_2 gas to the filtration cake and its residual solvent increases, which facilitates the evaporation of solvents in the filtration cake and thus drying. Second, the work from Huang and colleagues showed that increasing fluid pressure could change filtration cakes' structure, e.g., a cake can be compacted [10]. Such structure change, especially the relative movement of coal particles during the drying process, may help release liquid solvent initially trapped inside the cake's microcapillaries, thus enhancing drying.

Overall, the above results show that nitrogen with temperature up to 150°C and pressure up to 30 psig can reduce the cutoff drying time by ~50% compared to 20°C nitrogen tests. Despite the noticeable improvements, the drying time is still ~10 times longer than the 10 s required by the HHS technologies for coal dewatering.

3.2.3 Drying using superheated steam

Unable to produce satisfactory drying results using heated nitrogen, drying experiments using superheated steam as the drying medium and carrier gas were conducted. Figure 30 displays the drying curves obtained using 150°C superheated steam with a pressure of 5, 10, and 15 psig at the entrance of the drying vessel. Two key observations are that (1) superheated steam offers a significant improvement of drying performance over the heated N_2 with the same temperature and (2) increasing steam pressure from 5 to 15 psig greatly enhances the drying performance.

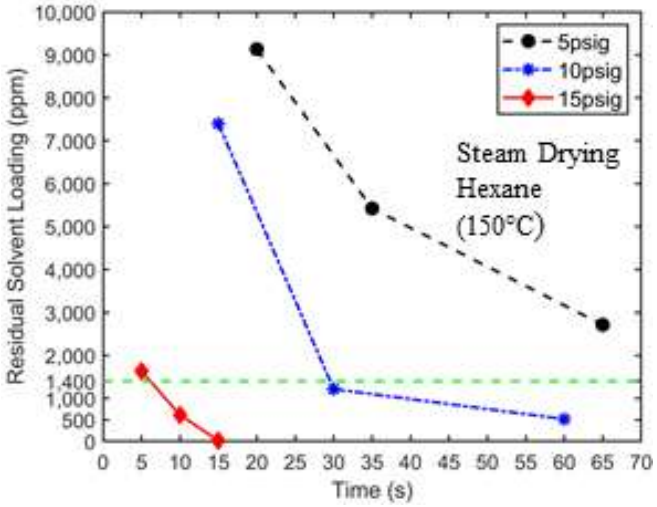

Figure 30: 150°C superheated steam drying curves at 5 psig, 10 psig, and 15 psig. The target solvent concentration of 1,400 ppm is denoted by a dashed horizontal line. The initial hexane loading is 24,500 ± 250 ppm.

Superheated steam offers much better drying performance over the heated N_2 with the same temperature. For 10 psig superheated steam, the target solvent concentration is reached at approximately 30 s. This drying result is in contrast to the fact that N_2 flow driven by twice the pressure difference (20 psig) did not reach the target concentration until approximately 130 s (see Figure 28). Furthermore, by reducing the solvent concentration to below 1400 ppm within approximately 6 s, the 15 psig superheated steam meets the requirement for HHS-based drying technology. It should be possible to optimize the steam pressure further so that the target solvent

concentration is reached at 10 s. However, this optimization is not pursued here since 15 psig steam provides a reasonable safety margin for drying time, which will be helpful in practical scale-up.

The much better drying performance of superheated steam over N_2 of the same temperature is attributed to the different drying mechanisms of these two carrier gases. Unlike N_2, when steam enters the filtration cakes at room temperature, it condenses rapidly. The heat thus released is significantly greater than that afforded by heated N_2. For example, when 150°C steams at 5, 10, and 15 psig condense into saturated liquids at the same pressure, their specific enthalpies decrease by 2320.8, 2289.1, and 2261.9 kJ/kg, respectively. On the other hand, even if 150°C N_2 is cooled to 20°C, its specific enthalpy decreases only by about 136.5 kJ/kg. As such, solvents are vaporized at a higher rate when steam is used, which facilitates the solvent removal from filtration cakes and results in faster drying. Conceivably, the condensation of water in the filtration cake can block some pores in the cake, trap liquid solvents, and slow down drying. However, the superior drying performance shown in Figure 30 suggests that these processes are not very significant.

For superheated steam, the drying rate increases significantly as its pressure increases from 5 to 15 psig. This can likely be attributed to the increased steam flow into the filtration cake as steam pressure increases, whose condensation facilitates the vaporization of solvents in the cake.

During the early stage of drying, the steam condenses on the inner surface of filtration cakes. Driven by the heat transfer from the superheated steam, the liquid condensates are later vaporized and removed from the filtration cake by convection. Because the ultimate goal of HHS technology and the present work is coal dewatering, it is necessary to determine the residual water content in the filtration cake at the end of drying. Tests were conducted on all three cake samples, and the water content was all below 5%. In the industrial handling of coal, the moisture content of coal is an important parameter to monitor because if coal becomes too dry, it can be a safety hazard. If it

is too wet, the heating value is reduced and can cause problems during transportation. Typical market specifications require coal moisture to be below 8% [2]. Therefore, the water content in coal dried here is acceptable. Further study of controlling moisture content by varying superheated steam temperatures and pressures can be conducted if more precise moisture control is required.

As shown in Figure 30, 10 psig and 5 psig steams with a temperature of 150°C are not able to reduce the solvent content in filtration cake to the target concentration within the desired 10 s time period. It is worthwhile to determine if higher superheat temperatures may address this limitation. Therefore, drying experiments were conducted with 5 psig steam at 180°C, the highest temperature that can be tolerated by our experimental apparatus. Figure 31 compares the 150°C 5 psig steam drying curve with that of the 5 psig 180°C steam to determine the benefit of raising superheat temperature while maintaining steam pressure. It is observed that, as the superheat increases by 30°C, the beginning part of the drying curve changes little. Drying with 180°C steam becomes faster than that with 150°C steam after the solvent concentration drops below ~5000 ppm, and the target solvent concentration is nearly reached at about 65 s. This, however, represents only a minor improvement compared to the drying with 150°C steam. Therefore, increasing the steam pressure rather than temperature is a more effective way to enhance drying, at least within the range of temperature and pressure explored in this work. Overall, 15 psig steam at 150°C is the best carrier gas studied in this study.

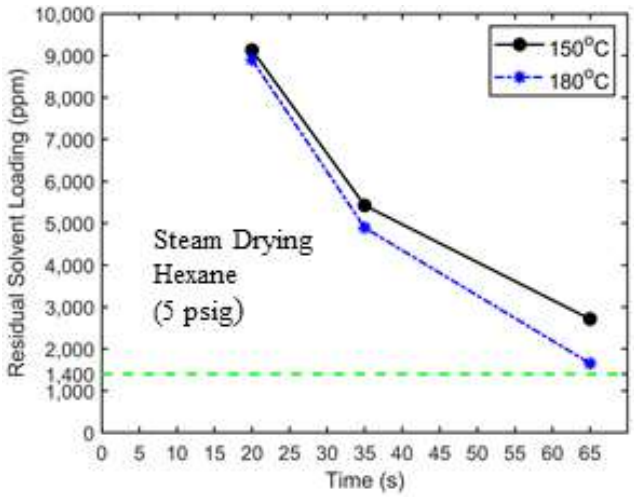

Figure 31: 5 psig superheated steam drying curves at 150°C and 180°C. The target solvent concentration of 1,400 ppm is denoted by a dashed horizontal line. The initial hexane loading is 24,500 ± 250 ppm.

All the above drying tests were conducted using filtration cakes prepared by pressure filtration of solvent-coal slurries (pressure difference: 20 psig). In commercial applications, filtration equipment is available in either a vacuum-type filter model or a high-pressure model. The latter can at times be significantly more expensive, and thus vacuum filtration is often preferred. However, in vacuum filtration, the available pressure difference for driving the formation of filtration cake is considerably lower than the atmosphere pressure (14.5 psia) and thus the 20 psig used in our pressure filtration work. As discussed earlier, Huang and colleagues showed that an increase in pressure while filtering a fine clay led to the cake being more compacted and having smaller pore radii [10]. Therefore, if a vacuum filter were used to form a fine coal cake, it would be expected to be less compact and have greater pore radii than a cake formed by 20 psig nitrogen. The effects that the cake formation method have upon cake structure may increase or decrease drying time. Therefore, it is desirable to investigate how drying would be affected if a vacuum filter forms the filtration cake.

Figure 32 compares the drying curves of filtration cakes formed by vacuum filtration and 20 psig nitrogen but dried using the same 15 psig and 150°C superheated steam. It is observed that,

with the filtration cake formed by vacuum filtration, the solvent content is reduced to the target concentration of 1400 ppm in approximately 9 s. While this represents a nearly 50% increase in drying time from the filtration cakes formed by N_2 pressure filtration, it is still below the target drying time of 10 s. The slower drying of vacuum-formed coal cakes suggests that a more tightly formed filtration cake promotes more efficient drying. This is likely caused by the fact that, in more tightly packed filtration cakes, the carrier gas flows more uniformly through the cake and thus, the transport of vaporized solvent to carrier gas streams is more facile. On the contrary, in loosely packed filtration cakes, the carrier gas may flow preferentially through a limited number of wide pores across the filtration cake. As a result, the vapor from liquid solvents trapped in tiny pores must travel a significant distance to reach the main carrier gas streams, hindering drying.

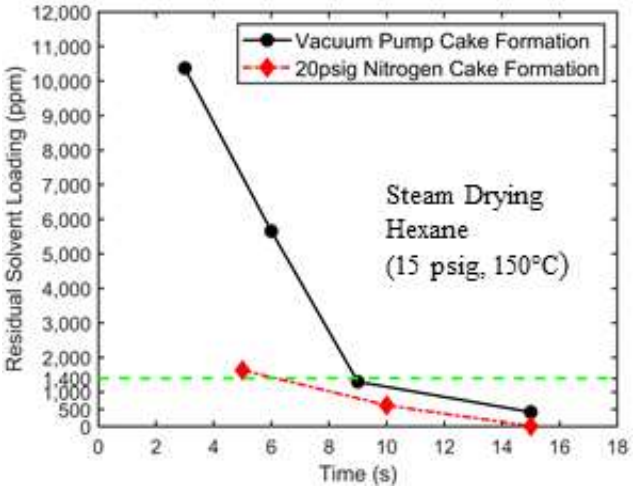

Figure 32: 15 psig, 150°C steam drying curves for vacuum-formed filtration cakes and 20 psig nitrogen-formed filtration cakes. The target solvent concentration of 1,400 ppm is denoted by a dashed horizontal line. The initial hexane loading is 24,500 ± 250 ppm.

Chapter 4. Conclusions

A recently developed technology called hydrophobic-hydrophilic separation (HHS) has been used to simultaneously clean and dewater fine coals. The HHS operations produce fine coal dispersed in hydrophobic solvents. To achieve economic viability, it is necessary to reduce the residual solvent concentration in produced coal to below 1400 ppm. In this work, an *in-situ* solvent recovery scheme is used to achieve this goal. The scheme includes a liquid-solid filtration stage to recover most solvents and a drying stage to reduce the solvent concentration to the target concentration. The drying stage immediately follows the filtration stage and involves the vaporization of solvents in the filtration cake and the subsequent removal through convection by a carrier gas. A series of experiments were carried out to identify filtration and drying operations that allow the solvent concentration to be reduced to the target concentration within the time required by the commercial application of the HHS technologies.

Our experiments showed that pressure filtration with 20 psig nitrogen could finish the filtration step in 60 s. Analysis aided by the classical model of mass convection in round pipes revealed that the residual solvents at the end of filtration exist in the form of isolated clusters trapped in small cavities that are sparsely distributed in the filtration cake. Room-temperature N_2 nor N_2 heated to 150°C, even at an elevated pressure of 30 psig, cannot reduce the solvent concentration in filtration cakes to the target concentration within 10 s. It is found that drying using 15 psig steam superheated to 150°C can reduce solvent concentration below 1400 pm in less than 10 s, and the water content in the final filtration cakes does not exceed the limit set for commercial clean coal. Increasing the temperature and pressure of superheated steam using a carrier gas does not markedly improve the drying performance. Even if filtration cakes are formed by vacuum filtration, which involves less

equipment cost but produces less compact cakes, drying can still be accomplished effectively with 15 psig steam superheated to 150°C.

The results and methods of this work can be further optimized and studied. First, it possible to explore using different superheated steam temperatures and pressures to control the final water content in the dried coal cake. This is desirable because the final preferred moisture content can vary depending on the future use of the coal. Second, it was discovered that a coal cake formed by a vacuum pump results in a slightly different drying time than that of a cake formed by 20 psig nitrogen. It would be worthwhile to study the effects of cake formation method and filtration pressure on drying time for a wider set of parameters.

Third, 15 psig 150°C steam was determined to be the optimal drying setting out of the options tested. This can be further refined by testing in between 10 psig and 15 psig, and by altering superheat temperature to determine a more precise drying setting arriving at an exact ten second drying time. Fourth, the simple model developed in this thesis was for isothermal room temperature drying. It would be helpful to develop a computational method for predicting superheated steam drying depending on temperature and pressure.

Fifth, the filtration and drying experimental apparatus used for this work prevented testing different cake depths. It would be useful to study filtration and drying on a number of thicker cakes. Additionally, this could include using different coal samples with different material properties, or even other minerals. Last, from rough calculations it is expected that using superheated steam as a drying medium will provide cost savings compared to currently utilized methods. Constructing an economic analysis of the HHS drying process will provide insight into the most sensitive cost parameters, and how the process can be optimized to further reduce energy use.

References

[1] EIA, "INTERNATIONAL ENERGY OUTLOOK 2021," in *Renewables will account for most global generation increases, but coal use remains high*, ed. eia.gov: EIA, 2021.

[2] N. Gupta, "Development of a novel fine coal cleaning and dewatering technology" Doctor of Philosophy, Mining and Minerals Engineering, Virginia Polytechnic Institute and State University, 2014.

[3] N. R. Council, *Coal Waste Impoundments: Risks, Responses, and Alternatives*. Washington, DC: The National Academies Press (in English), 2002, p. 242.

[4] R. H. Yoon, "Fine Coal Beneficiation Fine Coal Beneficiation and Recovery and Recovery," in *Workshop on Coal Beneficiation and Utilization of Rejects Initiatives, Policies and Practices*, 2007: Center for Advanced Separation Technologies.

[5] D. G. Osborne, *Coal Preparation Technology*. London, UK: Graham & Trotman Limited, 1988.

[6] R. Y. Jumah, "Dryer Emission Control System," in *Handbook of Industrial Drying*, A. S. Mujumdar Ed. Boca Raton: CRC Press, 2006, p. 1058.

[7] N. Gupta, B. li, G. Luttrell, R. H. Yoon, R. Bratton, and J. Reyher, *Hydrophobic-hydrophilic separation (HHS) process for the recovery and dewatering of ultrafine coal*. 2016.

[8] N. Gupta *et al.*, *HHS Process: A New Approach for Recovering Fine Illinois Basin Coals*. 2016.

[9] R.-H. Yoon, "Method for separating and de-watering fine particles," United States Patent 9,518,241, 2016.

[10] K. Huang, Pan, L., Yoon, R.H., "A capillary flow model for filtration," *Minerals Engineering,* vol. 115, pp. 88-96, 2018.

[11] R.-H. Yoon, "Methods of enhancing fine particle dewatering," U.S Patent 6,855,260, 2005.

[12] R.-H. Yoon, "Method for dewatering fine coal," U.S. Patent 5,458,786, 1995.

[13] E. U. Schlünder, "Drying of Porous Material During the Constant and the Falling Rate Period: A Critical Review of Existing Hypotheses," *Drying Technology,* vol. 22, no. 6, pp. 1517-1532, 2004/06/01 2004, doi: 10.1081/DRT-120038738.

[14] B. K. May, A. J. Sinclair, A. L. Halmos, and V. N. Tran, "Quantitative analysis of drying behaviour of fruits and vegetables," *Drying Technology,* vol. 17, no. 7-8, pp. 1441-1448, 1999, doi: 10.1080/07373939908917626.

[15] D. Chinweuba, N. Nwakuba, O. Chijioke, and C. Nwajinka, "Thin Layer Drying Modelling for Some Selected Nigerian Produce: A Review," vol. 3, pp. 1-15, 01/01 2016.

[16] T. Somjai, S. Achariyaviriya, A. Achariyaviriya, and K. Namsanguan, "Strategy for longan drying in two-stage superheated steam and hot air," *Journal of Food Engineering,* vol. 95, no. 2, pp. 313-321, 2009/11/01/ 2009, doi: https://doi.org/10.1016/j.jfoodeng.2009.05.005.

[17] A. Johansson, C. Fyhr, and A. Rasmuson, "High temperature convective drying of wood chips with air and superheated steam," *International Journal of Heat and Mass Transfer,* vol. 40, no. 12, pp. 2843-2858, 1997/08/01/ 1997, doi: https://doi.org/10.1016/S0017-9310(96)00341-9.

[18] S. Pang and M. Dakin, "Drying Rate and Temperature Profile For Superheated Steam Vacuum Drying and Moist AIr Drying of Softwood Lumber," *Drying Technology,* vol. 17, no. 6, pp. 1135-1147, 1999/05/01 1999, doi: 10.1080/07373939908917599.

[19] H. C. van Deventer, "Feasibility of energy efficient steam drying of paper and textile including process integration," *Applied Thermal Engineering,* vol. 17, no. 8, pp. 1035-1041, 1997/08/01/ 1997, doi: https://doi.org/10.1016/S1359-4311(97)00042-2.

[20] S. Soponronnarit, S. Prachayawarakorn, W. Rordprapat, A. Nathakaranakule, and W. Tia, "A Superheated-Steam Fluidized-Bed Dryer for Parboiled Rice: Testing of a Pilot-Scale and Mathematical Model Development," *Drying Technology,* vol. 24, no. 11, pp. 1457-1467, 2006/11/01 2006, doi: 10.1080/07373930600952800.

[21] H. C. van Deventer and R. M. H. Heijmans, "Drying With Superheated Steam," *Drying Technology,* vol. 19, no. 8, pp. 2033-2045, 2001/08/31 2001, doi: 10.1081/DRT-100107287.

[22] W. J. M. Douglas, "Drying Paper In Superheated Steam," *Drying Technology,* vol. 12, no. 6, pp. 1341-1355, 1994/01/01 1994, doi: 10.1080/07373939408961009.

[23] A. Speckhahn, G. Srzednicki, and D. K. Desai, "Drying of Beef in Superheated Steam," *Drying Technology,* vol. 28, no. 9, pp. 1072-1082, 2010/08/31 2010, doi: 10.1080/07373937.2010.505547.

[24] C. Pronyk, S. Cenkowski, and W. E. Muir, "Drying Foodstuffs with Superheated Steam," *Drying Technology,* vol. 22, no. 5, pp. 899-916, 2004/12/31 2004, doi: 10.1081/DRT-120038571.

[25] Y. B. Li, J. Seyed-Yagoobi, R. G. Moreira, and R. Yamsaengsung, "Superheated Steam Impingement Drying Of Tortilla Chips," *Drying Technology,* vol. 17, no. 1-2, pp. 191-213, 1999/01/01 1999, doi: 10.1080/07373939908917525.

[26] Q.-C. L. Jie Li, Lyes Bennamoun, "Superheated steam drying: Design aspects, energetic performances, and mathematical modeling," *Renewable and Sustainable Energy Reviews,* vol. 60, pp. 1562-1583, 2016.

[27] A. Bejan, *Convection Heat Transfer*. John Wiley & Sons, 2013.

[28] H. Shibata, "Comparison of Drying Rate Curves of Porous Solids in Superheated Steam to Those in Air," *Drying Technology,* vol. 23, no. 7, pp. 1419-1434, 2005/07/01 2005, doi: 10.1081/DRT-200063499.

[29] J. F. Bond, A. S. Mujumdar, A. R. P. van Heiningen, and W. J. M. Douglas, "Drying paper by impinging jets of superheated steam. Part 1: Constant drying rate in superheated steam," *The Canadian Journal of Chemical Engineering,* vol. 72, no. 3, pp. 446-451, 1994, doi: https://doi.org/10.1002/cjce.5450720309.

[30] A. Belhamri, "Characterization of the First Falling Rate Period During Drying of a Porous Material," *Drying Technology,* vol. 21, no. 7, pp. 1235-1252, 2003/01/08 2003, doi: 10.1081/DRT-120023178.